ASCE

Unified Compressive Strength and Strain Ductility Models for Fully and Partially FRP-Confined Circular, Square, and Rectangular Concrete Columns

Javad Shayanfar[1]; Joaquim A. O. Barros[2]; Mohammadmahdi Abedi[3]; and Mohammadali Rezazadeh[4]

Abstract: Determination of fiber-reinforced polymer (FRP) confinement-induced improvements in the mechanical properties of concrete columns under compression is a current concern, particularly if partial confinement applied on a noncircular cross-sectional shape is to be considered. Although several design-oriented predictive formulations have been proposed for the calculation of axial strength and axial strain ductility of FRP-confined concrete, their applications are, in general, limited to a specific cross-sectional shape (circular, square, or rectangular cross section) and a certain confinement arrangement (fully or partially confining system). Accordingly, the aim in this study is to establish new unified strength and ductility models for concrete columns of circular or noncircular cross sections with fully or partially confining FRP systems. To achieve the highest level of predictive performance through a nonlinear regression technique, two datasets, consisting of 2,117 test data of peak strength and 2,050 test data of strain ductility, available in the literature, were collected. The dominance degrees of size effect, sectional noncircularity (corner radius ratio), cross-sectional aspect ratio, and confinement configuration type on confinement effectiveness were evaluated and reflected in the development of these regression-based models. Through predictions of test data compiled in the datasets and a comparison with the performances of available predictive models, the proposed unified formulations demonstrated a high level of reliability and were found to be proper for design purposes. **DOI: 10.1061/JCCOF2.CCENG-4336**. © *2023 American Society of Civil Engineers*.

Author keywords: Unified model; Compressive strength; Axial strain ductility; Partial fiber-reinforced polymer (FRP) confinement; Noncircular cross section.

Introduction

The use of fiber-reinforced polymer (FRP) composites has become accepted for structural strengthening of concrete or reinforced concrete (RC) elements (Wang and Restrepo 2001; Pampanin et al. 2007; Barros et al. 2007; Triantafyllou et al. 2015; Teng et al. 2016; Wang et al. 2018a; Nematzadeh et al. 2021; Ma et al. 2023). Experimental studies (Harajli et al. 2006; Ozbakkaloglu and Vincent 2014; Shan et al. 2019) have clearly revealed that confinement provided by externally bonded FRP jackets is able to substantially improve the axial response of concrete material in terms of compressive strength, axial strain or deformation ductility, and energy dissipation. The basic principle in the performance of FRP-confined concrete columns is that FRP lateral pressure imposed to concrete is increased or activated by the transverse expansion of concrete under axial compressive loading, leading to a certain degree of enhancement in the confined concrete's response.

For fully FRP-confined circular concrete columns (labeled "FFCC" in Fig. 1), De Oliveira et al. (2019) experimentally demonstrated that FRP confinement-induced enhancements, in terms of axial strength and strain capacities, are strongly dependent on confinement stiffness (or FRP reinforcement ratio) and FRP rupture strain (De Oliveira et al. 2019). However, these improvements are dependent on the concrete strength, owing to its direct correlation with its transverse deformability. In fact, FFCC with normal-strength concrete results in more improvement than FFCC with high-strength concrete under an identical confinement stiffness level (Eid et al. 2009; Ozbakkaloglu and Akin 2012; Lin et al. 2021). Experimental evidence reported by Saleem et al. (2017) demonstrated that FRP effectiveness is by far less pronounced for noncircular cross-section columns than circular ones; this is caused by the detrimental influences of horizontal arching action and stress concentration at sectional edges. For the case of fully FRP-confined square concrete columns (labeled "FFSC" in Fig. 1), this loss of confinement-induced improvement, which is known generally as a noncircularity effect, depends strongly on the sectional corner radius ratio ($R_r = 2r/b$, in which r = corner radius; and b = section dimension), where FFSC with sharp edges ($R_r = 0$) experiences the greatest improvement loss (Wang and Wu 2008; Shan et al. 2019). Moreover, the axial and dilation responses of rectangular cross-section concrete elements with full confinement configuration (labeled "FFRC" in Fig. 1) are strongly dependent on the cross-sectional aspect ratio ($R_{ca} = h/b$, in which b = shorter dimension of the column's cross section; and h = longer dimension of the column's cross section), as well as R_r, where an insignificant effectiveness might be achieved for FFRC with a

[1]Ph.D. Candidate, ISISE, Dept. of Civil Engineering, Univ. of Minho, Azurém 4800-058, Guimarães, Portugal (corresponding author). ORCID: https://orcid.org/0000-0002-8331-2434. Email: arch3d.ir@gmail.com

[2]Full Professor, ISISE, IBS, Dept. of Civil Engineering, Univ. of Minho, Azurém 4800-058, Guimarães, Portugal. ORCID: https://orcid.org/0000-0003-1528-757X. Email: barros@civil.uminho.pt

[3]Ph.D. Candidate, ISISE, Dept. of Civil Engineering, Univ. of Minho, Azurém 4800-058, Guimarães, Portugal. ORCID: https://orcid.org/0000-0002-2920-9284. Email: mohammadmehdi.abedi@gmail.com

[4]Assistant Professor, Civil Engineering, Dept. of Mechanical and Construction Engineering, Northumbria Univ., Newcastle upon Tyne NE1 8ST, UK. ORCID: https://orcid.org/0000-0003-1411-0051. Email: mohammadali.rezazadeh@northumbria.ac.uk

Note. This manuscript was submitted on March 31, 2023; approved on August 2, 2023; published online on September 12, 2023. Discussion period open until February 12, 2024; separate discussions must be submitted for individual papers. This paper is part of the ***Journal of Composites for Construction***, © ASCE, ISSN 1090-0268.

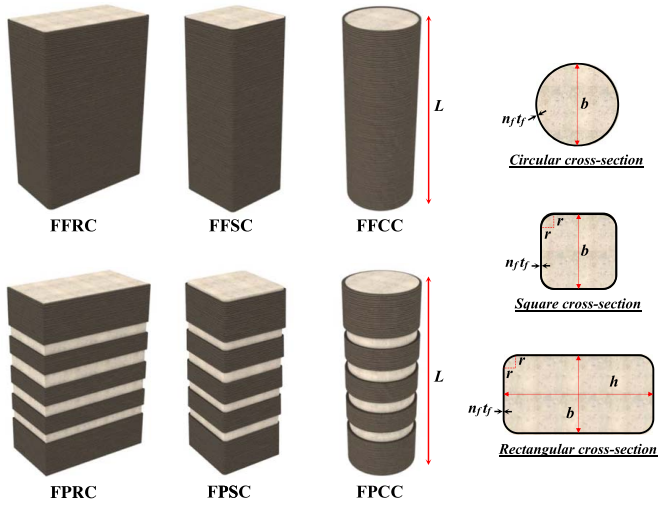

Fig. 1. Various confinement scenarios. FFRC = fully FRP-confined rectangular concrete column; FPRC = partially FRP-confined rectangular concrete column; FFSC = fully FRP-confined square concrete column; FPSC = partially FRP-confined square concrete column; FFCC = fully FRP-confined circular concrete column; FPCC = partially FRP-confined circular concrete column.

large R_{ca}, as experimentally evidenced by Ozbakkaloglu (2013), Triantafillou et al. (2016), Isleem et al. (2018) and Wang et al. (2021).

Considering the fact that a full confinement FRP strategy might not be cost-effective for strengthening applications, an alternative solution is to adopt a discontinuous confinement configuration. Barros and Ferreira (2008) experimentally verified that a sufficient level of load-carrying and axial strain or deformation ductility capacities can potentially be achieved by the consideration of discontinuous FRP strips between existing steel stirrups or hoops. For the case of partially FRP-confined circular concrete elements (labeled "FPCC" in Fig. 1), the confinement efficiency is reduced by increasing the distance between FRP strips (s_f), caused by vertical arching action and damage concentration in unwrapped zones. Experiments conducted by Zeng et al. (2017, 2018) showed that FRP confinement-induced improvements are more pronounced in FPCC than in noncircular cross-section columns with partial confinement (FPSC and FPRC, related to square and rectangular section, respectively, as shown in Fig. 1). Shayanfar et al. (2021a, 2022a) demonstrated that the axial and dilation responses of FPCC, FPSC, or FPRC with s_f larger than the damage zone length of unconfined concrete is almost the same as that in corresponding columns. It was also evidenced that above a certain limit of s_f, it is not useful to increase the FRP thickness, since this has a marginal effect on the column's confinement level.

To predict the response of FRP-confined concrete in terms of compressive strength and ultimate strain, a variety of predictive models has been suggested. These models can be categorized into three groups: (1) those developed based on an artificial intelligence (AI) approach (i.e., artificial neural networks) (Pham and Hadi 2014; Cascardi et al. 2017; Raza et al. 2022; Tariq et al. 2022; Isleem et al. 2022); (2) those developed based on multiple nonlinear or linear regression (Rousakis et al. 2012; Nisticò and Monti 2013; Cao et al. 2016; Shayanfar et al. 2022b; 2023d); and (3) those developed based on a hybrid approach, in which a powerful simulation tool, such as nonlinear finite-element analysis, is executed to provide additional information on significant but not experimentally measured parameters and also to enrich the extensiveness and quality of a test database through the generation of numerical data (Shayanfar et al. 2019; Fanaradelli and Rousakis 2020a, b). Owing to the capabilities of the AI approach in efficiently capturing the relationships between input variables, outputs, and their interactions, even for a very complex system, a more reliable model with high predictive performance can be established by AI in comparison with one developed based on regression analysis. Despite the merits of an AI approach over regression analysis, output obtained from regression analysis is as an algebraic or numerical equation, which is more easily implementable and also a more efficient technique for developing design-oriented predictive models than AI. Nonetheless, in the second and third categories, most of the regression-based developed equations have been developed exclusively for a specified cross-section shape or confining system.

It is noteworthy that a circular cross section can be considered as a special case of square cross section with $R_{ca} = 1$ and $R_r = 1$, as illustrated in Fig. 2. The square cross section itself can also be considered as a special case of rectangular cross section with $R_{ca} = 1$. Conversely, concrete columns with fully confining configuration can be recognized as a special case of a partial confinement arrangement, where s_f approaches zero ($s_f = 0$). Therefore, for various confinement scenarios (Fig. 1), the reliability of a nonunified model is at least arguable. Furthermore, owing to the lack of consistency, nonunified models do not lead to a smooth and reliable transition in their predictions from a circular cross section to a square or rectangular cross section or from full confinement to a partial confinement arrangement. To avoid discontinuity in the prediction caused by the alteration in cross-section shape and confining system, the development of a unified model, applicable to all these confinement scenarios, is necessary (Wei and Wu 2012). In general, for the case of cross-sectional and confining system unification, the concept of a "confinement efficiency factor" (Mander et al. 1988) is adopted by few models, for example, CNR DT 200/2004 (CNR 2004), Guo et al. (2018, 2019), and *fib* (2019), in which the influence of the arching action phenomenon is reflected empirically by a reduction factor in FRP confinement pressure, as the ratio of effective confinement area to the column entire area. Shayanfar et al. (2022b) modified the concept of a "confinement efficiency factor" proposed by Mander et al. (1988), by developing new theoretical-based formulations to simulate the influence of horizontal and vertical arching action phenomena in terms of peak compressive strength of FFSC, FPSC, or FPCC. A new definition of cross-sectional unification approach was introduced by Wu and Wang (2009), in which a unified strength model for square

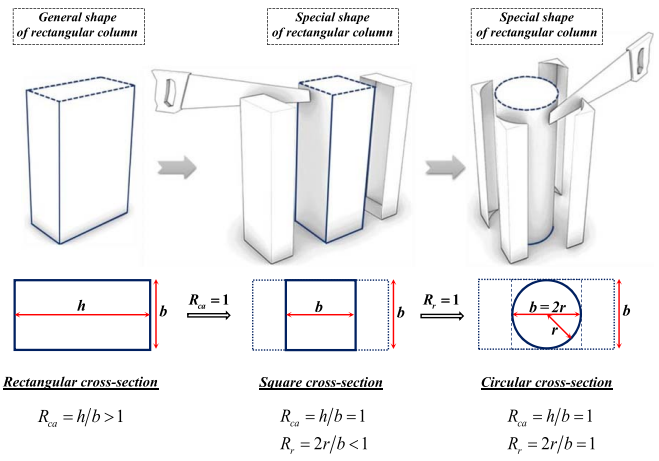

Fig. 2. Cross-sectional unification approach.

and circular cross-section concrete columns confined by FRP jackets (FFCC and FFSC) was proposed. In this approach, a unification factor was developed to reflect the influence of the noncircularity effect in model predictions based on the index of R_r, calibrated based on test results. By providing a larger test database of FFCC or FFSC for the model calibration, Shayanfar et al. (2023d) suggested a refined version of the model proposed by Wu and Wang (2009). By following the same approach, Wei and Wu (2012) extended this model (with some refinements) for the case of FFRC, where the index R_{ca} was used to reflect the effect of cross-sectional aspect ratio in reducing confinement effectiveness. Cao et al. (2016) improved Wei and Wu (2012)'s model by recalibrating its key components based on a larger test database. It was evidenced by Wu and Wang (2009), Wei and Wu (2012), and Shayanfar et al. (2023d) that, by following the methodology suggested by Wu and Wang (2009) based on a cross-sectional unification approach, rather than that suggested by the concept of a "confinement efficiency factor" of Mander et al. (1988), a more reliable and accurate predictive formulations could be derived for FFCC, FFSC, or FFRC. However, the reliability of generalizing Wu and Wang (2009)'s methodology for confining system unification (FPCC, FPSC, or FPRC) still requires demonstration. This is one of the main objectives of this study.

Conversely, in general, a regression analysis technique is adopted to unavoidably establish the relationship of key variables (i.e., FRP and concrete properties, specimen geometry, sectional aspect ratio, corner radius, FRP strip distance) with compressive strength and strain ductility capacities. Although the reliability of a regression-based developed model is strongly dependent on the extensiveness and quality of the database used, the majority of existing models were built on databases with limited data frequency covering a relatively short range of the key variables. Hence, the predictive performance of such models tends to degrade noticeably when a larger database is considered for statistical assessment (Ozbakkaloglu and Lim 2013). Considering the great number of experimental research studies conducted on the mechanical behavior of FRP-confined concrete columns in the past two decades, a large amount of experimental data is available in the literature. Accordingly, by gathering experimental data that was not available at the time of the data collection of existing databases, up-to-date databases for peak compressive strength and strain ductility capacities can potentially be collected. Accordingly, once these databases are available, a more reliable predictive model, with a superior performance to that associated with existing models, can be developed, which is also one of the main objectives of this study. It is also rational to have a continuous process of data collection and consequent recalibration of models until convergence in terms of accuracy is reached.

In this study, for the estimation of the compressive strength (f_{cc}) and strain ductility ($\mu_\varepsilon = \varepsilon_{cu}/\varepsilon_{c0}$, where ε_{c0}= axial strain corresponding to f_{c0}) of FRP-confined concrete specimens, new models were developed. These models were built based on the unification approach introduced by Wu and Wang (2009) through a multiple nonlinear regression technique performed on up-to-date and comprehensive test datasets. These datasets consisted of 2,117 and 2,050 experimental data available in the literature obtained from axial compressive tests, respectively, for peak strength and strain ductility of concrete columns. Furthermore, a new regression-based framework was derived based on the Poisson's ratio effect for the establishment of the proposed strain ductility model. Initially, regression-based predictive models were developed for the ultimate condition of FFCC. Subsequently, to simulate cross-section variation from circular (FFCC) to square (FFSC) or rectangular (FFRC) cross-section shape, the dominance degree of the corner radius ratio (R_r) and the cross-sectional aspect ratio (R_{ca}) were determined based on statistical assessment, and their influences on the models of f_{cc} and μ_ε were reflected. Besides cross-sectional unification, the transformation of the confining system from a fully (FFCC, FFSC, FFRC) to a partially (FPCC, FPSC, FPRC) confining system was considered by reflecting the impact of FRP strip distance to column dimension ratio ($R_{sf} = s_f/b$) in the cross-sectional unified model. The predictive performance of the proposed unified models was verified and also compared with some existing models.

Test Databases

A vital necessity for the development of an analytical-based predictive model is to collect the relative test database, including input and output variables. Several databases (De Lorenzis and Tepfers 2003; Nisticò and Monti 2013; Ozbakkaloglu and Lim 2013; Fanaradelli and Rousakis 2021; Isleem et al. 2022) have been provided for the case of compressive strength, f_{cc}, and axial strain ductility, μ_ε, of FRP-confined concrete. A review of the available databases reveals that a large amount of experimental data can still be added to these databases, evidently not available at the time of the data collection. Furthermore, they are applicable to either a specific cross-section shape (circular, square, or rectangular cross section) or a certain confinement arrangement (fully or partially confining system).

In this study, to develop predictive models for f_{cc} and μ_ε, two series of datasets were collected from axial compressive tests performed on FRP-confined concrete columns. The statistical information of key variables involved in these compiled test datasets is given in Tables 1 and 2.

The criteria considered for data collection, to produce systematically consistent datasets, were as follows:

1. Specimens with internal steel reinforcements were not included.
2. Only specimens with FRP confining systems in the hoop direction were included, and those with other types of confinement configuration, for example, hybrid or helical confining systems, were excluded.
3. Data from experiments with inadequately reported details, i.e., material and geometry properties, were excluded.
4. FRP-confined specimens with a peak strength (f_{cc}) less than the compressive strength of unconfined concrete (f_{c0}), representing no FRP confinement-induced improvement, were excluded.
5. Noncircular specimens with a corner radius ratio less than 0.05 ($R_r < 0.05$) were excluded. In fact, the confinement-induced improvements in such cases were marginal, owing to horizontal arching action and stress concentration at sectional edges. It should be noted that, in many practical situations for axial strengthening of real cases of large-scale RC columns, a relatively short radius of the rounded corners ($R_r \le 0.3$) is considered, owing to the limitations caused by internal steel reinforcements and the small thickness of concrete cover. The refinement of FRP confinement strategies for strengthening such cases is still an ongoing concern, as different solutions have been suggested to increase the effectiveness of FRP confinement. More information regarding these solutions can be found in Rousakis and Tourtouras (2014), Triantafillou et al. (2016), Janwaen et al. (2019), and He and Zeng (2022).
6. Noncircular specimens with a cross-sectional aspect ratio more than 3 ($R_{ca} > 3$) were excluded. This criterion was considered based on test results conducted by Pantelides et al. (2004) and Triantafillou et al. (2016).
7. Partially confined specimens with a FRP strip distance more than 0.75 times the shortest dimension of the column's cross section ($R_{sf} > 0.75$) were excluded. It should be noted that, based on Wei and Wu (2016), Wu and Wei (2016), and

Table 1. Summary of compiled test databases for compressive strength

Confinement arrangement	Number of datasets	Statistical indicator	f_{c0} (MPa)	f_{cc}/f_{c0}	L (mm)	b (mm)	E_f (GPa)	ε_{fu}	R_r	R_{ca}	R_{sf}
FC or PC	2,117	Min.	6.6	1.01	100	50	9.5	0.004	0.07	1	0
		Max.	204	6.90	1,200	400	657	0.100	1	3	0.75
		Mean	43.4	1.91	330	149	181	0.023	0.87	1.05	0.03
		CoV	0.684	0.423	0.401	0.291	0.522	0.793	0.307	0.200	3.591
FC	1,918	Min.	6.6	1.03	100	50	9.5	0.004	0.07	1	0
		Max.	204	6.90	1,200	400	657	0.100	1	3	0
		Mean	44.5	1.95	325	148	176	0.024	0.87	1.06	0
		CoV	0.689	0.422	0.405	0.298	0.585	0.806	0.310	0.209	—
PC	199	Min.	12.4	1.01	200	100	73	0.013	0.12	1	0.05
		Max.	101.2	3.58	750	300	260	0.028	1.00	1.54	0.75
		Mean	32.5	1.50	376	159	230	0.017	0.906	1.004	0.31
		CoV	0.413	0.296	0.343	0.213	0.163	0.112	0.270	0.043	0.553

Note: FC = full confinement; PC = partial confinement; f_{cc} = axial compressive strength of FRP-confined concrete; f_{c0} = axial compressive strength of unconfined concrete; L = height of column; b = section dimension; E_f = FRP modulus elasticity; ε_{fu} = FRP ultimate tensile strain.

Shayanfar et al. (2021a, 2023a), in partially confined specimens with an FRP strip distance longer than the damage zone length of unconfined concrete columns, the effect of partial confinement in restraining the local failure would be quite marginal. In such partially confined specimens, the axial response is controlled significantly by failure localization and concrete crushing in unwrapped zones (Wei and Wu 2016; Shayanfar et al. 2020). Accordingly, in this study, to have consistent datasets and filter out improper data, based on experimental observations (Zeng et al. 2017, 2018; Wang et al. 2018b), $R_{sf} = 0.75$ was assumed as a threshold beyond which confinement-induced improvements are almost negligible.

Based on test data available in the literature, for the compressive strength-related dataset, 2,117 data were collected, consisting of 1,918 data obtained from circular, square, or rectangular specimens with FRP full confinement configuration (FC), and 199 data obtained from FRP partially confined concrete (PC) of circular, square, or rectangular cross section. Furthermore, for the ultimate axial strain-related dataset, 2,050 data were collected, including 1,866 data of FC and 184 PC configurations. As given in Tables 1 and 2, these datasets provide not only a broad range of main input or output variables, but also a large data frequency.

It is clear that for concrete specimens with a sufficient level of FRP confinement (showing a monotonically ascending axial response), the ultimate axial strain (ε_{cu}) corresponds to the peak strength stage (f_{cc}) at the rupture of the FRP jacket. Nevertheless, specimens with an insufficient confinement (particularly noncircular columns or columns made of high-strength concrete) tend to reveal a strain softening postpeak behavior, where the ultimate stage (f_{cu}) at ε_{cu} occurs beyond the peak stage ($f_{cu} < f_{cc}$), as experimentally evidenced by Triantafillou et al. (2016) and De Oliveira et al. (2019). Accordingly, to have systematic consistency in the data collection, for specimens $f_{cu} \leq f_{cc}$, in this study, a criterion for ultimate condition was considered based on the recommendations of Teng et al. (2009) and Fanaradelli and Rousakis (2021). Accordingly, for specimens having strain softening postpeak behavior with $f_{cu} < 0.85 f_{cc}$, ε_{cu} was defined as the axial strain corresponding to 85% of f_{cc} in the descending branch of the axial stress–strain curve. Note that, for the calculation of ε_{c0} as an input parameter in $\mu_\varepsilon = \varepsilon_{cu}/\varepsilon_{c0}$, the formulation suggested by Shayanfar et al. (2023b) was followed as $\varepsilon_{c0} = 0.0011(f_{c0}b/L)^{0.25}$.

These provided datasets (Tables 1 and 2) contain test data from FRP-confined specimens with various kinds of FRP material, namely, carbon FRP (CFRP), glass FRP (GFRP), basalt FRP (BFRP), and aramid FRP (AFRP), as well as polyethylene naphthalate (PEN) and polyethylene terephthalate (PET) fibers. Note that, unlike conventional FRPs, PET and PEN FRPs have a nonlinear relationship between tensile stress and axial strain, providing a large ultimate tensile strain, over 5% (but with a relatively low level of initial elastic modulus), which considerably improves the columns' response in terms of ductility (Bai et al. 2014; Zeng et al. 2020). Dai et al. (2011) and Shayanfar et al. (2022b, 2023d) demonstrated that analysis or design-oriented models, established exclusively for cases with conventional FRPs (CFRP, GFRP, BFRP, AFRP) can

Table 2. Summary of compiled test databases for strain ductility

Confinement arrangement	Number of datasets	Statistical indicator	f_{c0} (MPa)	$\varepsilon_{cu}/\varepsilon_{c0}$	L (mm)	b (mm)	E_f (GPa)	ε_{fu}	R_r	R_{ca}	R_{sf}
FC or PC	2,050	Min.	6.6	1.10	100	50	9.5	0.004	0.07	1	0
		Max.	204	93.9	1,200	400	657	0.100	1	3	0.75
		Mean	44.1	10.1	330	148	179	0.023	0.87	1.06	0.03
		CoV	0.677	0.930	0.398	0.290	0.559	0.798	0.310	0.212	3.700
FC	1,866	Min.	6.6	1.22	100	50	9.5	0.004	0.07	1	0
		Max.	204	93.9	1,200	400	657	0.100	1	3	0
		Mean	45.1	10.3	327	147	174	0.024	0.87	1.06	0
		CoV	0.682	0.939	0.406	0.299	0.592	0.809	0.314	0.220	—
PC	184	Min.	16.6	1.10	200	100	105	0.013	0.12	1	0.05
		Max.	101.2	21.4	700	300	260	0.019	1.00	1.54	0.75
		Mean	33.8	7.76	360	155	230	0.017	0.909	1.004	0.32
		CoV	0.422	0.621	0.312	0.196	0.147	0.084	0.266	0.045	0.563

Note: FC = full confinement; PC = partial confinement; ε_{c0} = axial strain corresponding to f_{c0}.

also be adopted for those with PET or PEN FRPs through recalibration of the terms related to ultimate tensile strain and initial elastic modulus. Accordingly, in this study, data available in the literature from FRP-confined specimens with PET or PEN FRP jackets were included in these provided datasets.

It should be noted that, by using the assembled databases covering various kinds of FRP material, confinement-induced improvements in f_{cc} and ε_{cu} can be evaluated more widely with respect to the mechanical characteristics of FRP sheets (i.e., ε_{fu} and E_f), than those databases including only a specific type of FRP sheet. Furthermore, as can be seen in Tables 1 and 2, these databases also contain a wide range of values for the key variables concerning geometry (small, medium, and large specimens), and concrete properties (low-, normal-, high-, and ultrahigh-strength concrete). Thus, by adopting these assembled datasets, more reliable formulations for the calculation of f_{cc} and ε_{cu} can be built by using a regression analysis technique, in comparison with those predictive models calibrated using a series of test data with a limited range of values for the main variables.

Some Existing Models

Table 3 gives predictive formulations suggested by CNR DT 200/2004 (CNR 2004), Wei and Wu (2012), Cao et al. (2016), ACI 440.2R-17 (ACI 2017), Guo et al. (2018, 2019), and *fib* (2019) for the estimation of FRP-confined concrete's axial response in terms of f_{cc}/f_{c0} and $\mu_\varepsilon = \varepsilon_{cu}/\varepsilon_{c0}$. To develop predictive equations for f_{cc}/f_{c0}, these models assumed different methodologies, which can be categorized as follows:

1. relation development of f_{cc}/f_{c0} with $f_{l,\text{rup}}/f_{c0}$, where $f_{l,\text{rup}}$ is the confinement pressure imposed on the confined concrete corresponding to FRP rupture strain (CNR DT 200/2004 CNR 2004; ACI 2017; and *fib* 2019);
2. relation development of f_{cc}/f_{c0} with $f_{l,u}/f_{c0}$, where $f_{l,u}$ is the confinement pressure corresponding to FRP ultimate tensile strain (Wei and Wu 2012);
3. relation development of f_{cc}/f_{c0} with ρ_{Ke1} (normalized effective FRP confinement stiffness) and ρ_ε (rupture strain ratio of FRP jackets) (Guo et al. 2018, 2019);
4. relation development of f_{cc}/f_{c0} with key influential variables (Cao et al. 2016).

From an applicability point of view, the models presented by CNR DT 200/2004 (CNR 2004), Guo et al. (2018, 2019), and *fib* (2019) are applicable to all cases of FFCC, FFSC, FFRC, FPCC, FPSC, and FPRC, where the significant impact of arching action is considered based on the confinement efficiency factor (k_h and k_v, respectively), as originally suggested by Mander et al. (1988). However, the models suggested by Wei and Wu (2012), Cao et al. (2016), and ACI 440.2R-17 (ACI 2017) are applicable only to cases with a full confinement system (FFCC, FFSC, FFRC), where the cross-sectional shape effect is reflected (1) by using k_h (ACI 2017) or (2) by taking into account the dominance degree of R_r and R_{ca}, based on statistical analysis techniques (Wei and Wu 2012; Cao et al. 2016).

Conversely, the general structure of existing models for the establishment of $\mu_\varepsilon = \varepsilon_{cu}/\varepsilon_{c0}$ through the regression analysis technique can be expressed as

$$\mu_\varepsilon = \frac{\varepsilon_{cu}}{\varepsilon_{c0}} = k_0 + \Psi_c \tag{1}$$

where k_0 is a constant coefficient, suggested as 1.5 or 1.75, while Ψ_c is the term considered to determine the improvement induced by the FRP confinement system as a function of key influential variables (i.e., $f_{l,u}$, $f_{l,\text{rup}}$, K_L, f_{c0}, and ε_{fu}). Although the model developed by CNR DT 200/2004 (CNR 2004) and *fib* (2019) adopted the original concept of a confinement efficiency factor (k_h and k_v), a modified version of this concept was adopted by Guo et al. (2018, 2019) and ACI 440.2R-17 (ACI 2017) by adding empirical terms dependent on R_{ca}. For cross-sectional unification, Wei and Wu (2012) and Cao et al. (2016) considered R_r and R_{ca} in their models, based on a statistical analysis approach.

Determination of f_{cc} of FRP-Confined Concrete Columns

This section presents the determination of the proposed regression-based predictive model to derive the axial compressive strength (f_{cc}) of FRP-confined concrete under axial compressive loading. For this purpose, firstly, for the case of FFCC, a strength model considering the size effect, whose input variables are calibrated through a regression analysis technique performed on 1,517 experimental results, is developed. Then, this model is extended to cases of FFSC and FFRC by reflecting the influences of the noncircularity effect and sectional aspect ratio in terms of confinement effectiveness, calibrated based on 401 test specimens. The strength model is subsequently generalized for cases with partial confinement arrangement (FPCC, FPSC, and FPRC), where the dominance degree of partially imposed confinement is considered based on 199 experimental results for the calibration.

The methodology considered in this study for the application of the cross-sectional unification approach is as follows:

1. establishment of a predictive formulation for FFCC, calibrated using the collected database of FFCC specimens ($R_{ca} = 1$ and $R_r = 1$);
2. determination of the relationship of the error obtained from this model applied on FFSC specimens with respect to R_r in the range $0 \le R_r < 1$ (Tables 1 and 2);
3. generalization of the preliminary model for FFSC by using error analysis so that the generalized model could accurately provide a uniform predictive performance for all ranges of R_r;
4. determination of the relationship of the error obtained from the generalized model applied on FFRC specimens with respect to R_{ca} in the range $1 < R_{ca} \le 3$ (Tables 1 and 2);
5. generalization of the previous model for FFRC by using error analysis so that it could provide accurately a uniform performance for all ranges of R_r and R_{ca}.

Therefore, for concrete columns with FC, the effects of noncircularity and cross-sectional aspect ratio are formulated by error analyses of the model performance with R_{ca}.

For application of the confining system unification approach, the considered methodology is as follows:

1. determination of the relationship of the error obtained from the model generalized for FFCC, FFSC, FFRC (FC) applied on FPCC, FPSC, FPRC (PC) specimens with respect to R_{sf} in the range $0.05 \le R_{sf} \le 0.75$;
2. generalization of the previous model for PC specimens using the error analysis so that it could accurately provide a uniform predictive performance for all ranges of R_{sf}.

Accordingly, by formulating the effect of R_{sf}, the model could be applicable to various confinement scenarios (FFCC, FFSC, FFRC, FPCC FPSC, FPRC).

FFCC Column Elements

In this study, to calculate confinement lateral pressure ($f_{l,\text{rup}}$) at FRP rupture hoop strain ($\varepsilon_{h,\text{rup}}$) imposed on the concrete of FFCC,

Table 3. Existing models recommended for prediction of peak strength and axial strain ductility of FRP-confined concrete

ID	Model expression		Model parameters	Applicability
	Compressive strength	Axial ductility		
fib (2019)	$\frac{f_{cc}}{f_{c0}} = 1 + 3.3\frac{f_{l,\text{rup}}}{f_{c0}}$ for $\frac{f_{l,\text{rup}}}{f_{c0}} \geq 0.07$ $\frac{f_{cc}}{f_{c0}} = 1$ for $\frac{f_{l,\text{rup}}}{f_{c0}} \leq 0.07$	$\mu_\varepsilon = 1.75 + 12\sqrt{\frac{h}{b}}\frac{f_{l,\text{rup}}}{f_{c0}}\left(\frac{\varepsilon_{h,\text{rup}}}{\varepsilon_{c0}}\right)^{0.45}$	$f_{l,\text{rup}} = 2K_e\frac{n_f t_f E_f}{D^*}\varepsilon_{h,\text{rup}}$ for $n_f \leq 3$ $f_{l,\text{rup}} = 2K_e\frac{n_f^{0.85} t_f E_f}{D^*}\varepsilon_{h,\text{rup}}$ for $n_f \geq 4$ $D^* = \frac{2bh}{b+h}$ $K_e = k_h k_v$ $k_h = 1 - \frac{(b-2r)^2 + (h-2r)^2}{3bh}$ $k_v = \left(1 - \frac{s_f}{2b}\right)\left(1 - \frac{s_f}{2h}\right)$ $\varepsilon_{h,\text{rup}} = \eta_e \varepsilon_{fu}$ $\eta_e = 0.5\frac{r}{50}\left(2 - \frac{r}{50}\right)$ for $r \leq 60$ mm $\eta_e = 0.5$ for $r > 60$ mm	FFCC FFSC FFRC FPCC FPSC FPRC
CNR DT 200/2004 (CNR 2004)	$\frac{f_{cc}}{f_{c0}} = 1 + 2.6\left(\frac{f_{l,\text{rup}}}{f_{c0}}\right)^{\frac{2}{3}}$ for $\frac{f_{l,\text{rup}}}{f_{c0}} \geq 0.05$ $\frac{f_{cc}}{f_{c0}} = 1$ for $\frac{f_{l,\text{rup}}}{f_{c0}} \leq 0.05$	$\mu_\varepsilon = 1.75 + 7.5\sqrt{\frac{f_{l,\text{rup}}}{f_{c0}}}$	$f_{l,\text{rup}} = \frac{1}{2}K_e\rho_f E_f \varepsilon_{fd.rid}$ $\rho_f = \frac{4n_f t_f}{b}$ for FFCC $\rho_f = \frac{2n_f t_f (b+h)}{bh}$ for FFSC, FFRC $\rho_f = \frac{4n_f t_f w_f}{bs_f}$ for FPCC $\rho_f = \frac{2n_f t_f (b+h) w_f}{bhs_f}$ for FPSC, FPRC $K_e = k_h k_v$ $k_h = 1 - \frac{(b-2r)^2 + (h-2r)^2}{3bh}$ $k_v = \left(1 - \frac{s_f}{2b}\right)\left(1 - \frac{s_f}{2h}\right)$ $\varepsilon_{fd.rid} = \min\left\{\frac{\eta_a \varepsilon_{fu}}{\lambda_f}, 0.004\right\}$ $\eta_a = 0.65$, 0.75 and 0.85 for the fiber resin type: glass/epoxy, aramid/epoxy, carbon/epoxy, respectively. $\lambda_f =$ partial factor recommended as 1.10.	FFCC FFSC FFRC FPCC FPSC FPRC

Table 3. (*Continued.*)

ID	Model expression		Model parameters	Applicability
	Compressive strength	Axial ductility		
Guo et al. (2018, 2019)	$\frac{f_{cc}}{f_{c0}} = 1 + 2(\rho_{Ke1} - 0.01)\rho_\varepsilon$ for $\rho_{Ke1} \geq 0.01$ $\frac{f_{cc}}{f_{c0}} = 1$ for $\rho_{Ke2} \leq 0.01$	$\mu_\varepsilon = 1.75 + 5.5\rho_{Ke2}^{0.8}\rho_\varepsilon^{1.45}$	$\rho_{Ke1} = 2K_{e1}\frac{n_f t_f E_f \varepsilon_{c0}}{D^* f_{c0}}$ $\rho_{Ke2} = 2K_{e2}\frac{n_f t_f E_f \varepsilon_{c0}}{D^* f_{c0}}$ $\rho_\varepsilon = \frac{\varepsilon_{h,\text{rup}}}{\varepsilon_{c0}}$ $D^* = b$ for circular $D^* = \sqrt{b^2 + h^2}$ for noncircular $K_{e1} = \left(\frac{b}{h}\right)^2 k_h k_v$ $K_{e2} = \left(\frac{h}{b}\right)^{0.5} k_h k_v$ $k_h = 1 - \frac{\frac{h}{b}(b-2r)^2 + \frac{b}{h}(h-2r)^2}{3bh}$ $k_v = \left(1 - \frac{s_f}{2b}\right)\left(1 - \frac{s_f}{2h}\right)$ $\varepsilon_{h,\text{rup}} = 0.568\varepsilon_{fu}$	FFCC FFSC FFRC FPCC FPSC FPRC
ACI440.2R-17 (ACI 2017)	$\frac{f_{cc}}{f_{c0}} = 1 + 3.3\psi_f \frac{f_{l,\text{rup}}}{f_{c0}}$ for $\frac{f_{l,\text{rup}}}{f_{c0}} \geq 0.08$ $\frac{f_{cc}}{f_{c0}} = 1$ for $\frac{f_{l,\text{rup}}}{f_{c0}} \leq 0.08$	$\mu_\varepsilon = 1.5 + 12\sqrt{\frac{h}{b}}\frac{f_{l,\text{rup}}}{f_{c0}}\left(\frac{\varepsilon_{h,\text{rup}}}{\varepsilon_{c0}}\right)^{0.45}$	$f_{l,\text{rup}} = 2K_e\frac{n_f t_f E_f}{D^*}\varepsilon_{h,\text{rup}}$ $D^* = b$ for FFCC $D^* = \sqrt{b^2 + h^2}$ for FFSC, FFRC $K_e = k_h k_v$ $k_h = 1 - \frac{\frac{h}{b}(b-2r)^2 + \frac{b}{h}(h-2r)^2}{3bh}$ $k_v = \left(1 - \frac{s_f}{2b}\right)\left(1 - \frac{s_f}{2h}\right)$ $\varepsilon_{h,\text{rup}} = 0.55\varepsilon_{fu}$	FFCC FFSC FFRC
Cao et al. (2016)	$\frac{f_{cc}}{f_{c0}} = 1 + 8.34\left(\frac{K_L}{E_c}\right)^{1.03}\left(\frac{2r}{b}\right)^{0.81}\left(\frac{30}{f_{c0}}\right)^{0.54}\left(\frac{h}{b}\right)^{-1.9}\left(\frac{\varepsilon_{fu}}{\varepsilon_{c0}}\right)^{0.82}$	$\mu_\varepsilon = 1.75 + 9.45k_R\left(\frac{K_L}{E_c}\right)^{0.68}\left(\frac{30}{f_{c0}}\right)^{0.79}\left(\frac{h}{b}\right)^{-0.64}\left(\frac{\varepsilon_{fu}}{\varepsilon_{c0}}\right)^{1.14}$	$k_R = 0.54R_r + 0.46$ $K_L = 2\frac{n_f t_f E_f}{b}$ $E_c = 4730\sqrt{f_{c0}}$	FFCC FFSC FFRC
Wei and Wu (2012)	$\frac{f_{cc}}{f_{c0}} = 1 + 2.2\left(\frac{2r}{b}\right)^{0.72}\left(\frac{h}{b}\right)^{-1.9}\left(\frac{f_{l,u}}{f_{c0}}\right)^{0.94}$	$\mu_\varepsilon = 1.75 + 12(0.36R_r + 0.64)\left(\frac{f_{l,u}}{f_{c0}}\right)^{0.75}\left(\frac{30}{f_{c0}}\right)^{0.62}\left(\frac{h}{b}\right)^{-0.3}$	$f_{l,u} = 2\frac{n_f t_f E_f}{b}\varepsilon_{fu}$	FFCC FFSC FFRC

Note: f_{cc} = axial compressive strength of FRP-confined concrete; f_{c0} = axial compressive strength of unconfined concrete; $f_{l,\text{rup}}$ = confinement pressure corresponding to FRP rupture strain ($\varepsilon_{h,\text{rup}}$); $f_{l,u}$ = FRP confinement pressure at ultimate tensile strain (ε_{fu}); n_f = number of FRP layers; t_f = nominal FRP thickness; k_h = confinement efficiency factor reflecting the effect of horizontal arching action; k_v = confinement efficiency factor reflecting the effect of vertical arching action; ρ_f = FRP reinforcement ratio; ρ_{Ke} = effective FRP confinement stiffness index; ρ_ε = FRP strain ratio; ε_{c0} = axial strain corresponding to f_{c0}; ψ_f = reduction factor recommended as 0.95; K_L = FRP confinement stiffness per length of section dimension; E_c = concrete modulus of elasticity.

fib (2019)'s recommendation is followed:

$$f_{l,\text{rup}} = 2\frac{n_f^{\kappa} t_f E_f}{b}\varepsilon_{h,\text{rup}} = K_L \varepsilon_{h,\text{rup}} \tag{2}$$

in which

$$K_L = 2\frac{n_f^{\kappa} t_f E_f}{b} \qquad (\text{in MPa, and } t_f \text{ and } b \text{ in mm}) \tag{3}$$

where n_f = number of FRP layers; $\kappa = 1$ and 0.85, corresponding to $n_f \le 3$ and $n_f \ge 4$, respectively; t_f = nominal thickness of a FRP layer; E_f = FRP elasticity modulus; and K_L = FRP confinement stiffness. In general, $\varepsilon_{h,\text{rup}}$ is assumed to be a constant percentage of the ultimate tensile strain of the FRP sheet (ε_{fu}), i.e., $\varepsilon_{h,\text{rup}} = \psi\varepsilon_{fu}$, where $\psi < 1$ is generally known as a strain reduction factor (Lam and Teng 2003). However, studies (Lim and Ozbakkaloglu 2014 ; Shayanfar et al. 2020) demonstrated that ψ is affected by the concrete strength (f_{c0}) and the type of FRP material (E_f or ε_{fu}). However, through a probabilistic procedure implemented on a large database of $\varepsilon_{h,\text{rup}}$, Baji et al. (2016) suggested $\psi = 0.68$ by ignoring the influences of f_{c0} and E_f on ψ, owing to a relatively low correlation obtained between these variables. Accordingly, in this study, for the sake of simplicity, based on Baji et al. (2016)'s recommendation, ψ was considered constant (i.e., 0.68). It is noteworthy that the possible level of error caused by this simplification can be minimized during regression analysis where the developed formulations are built based on ε_{fu} rather than $\varepsilon_{h,\text{rup}}$ (Rousakis et al. 2012). More information regarding the strain reduction factor can be found in Wu and Jiang (2013) and Lim and Ozbakkaloglu (2014).

For FRP-confined circular cross-section concrete columns under axial loading, owing to the confinement imposed on the concrete, a certain level of enhancement (Δ_c) in terms of axial compressive strength (f_{cc}) is achieved. Accordingly, f_{cc}/f_{c0} of FFCC can be expressed as

$$\frac{f_{cc}}{f_{c0}} = 1 + \Delta_c \tag{4}$$

In general, Δ_c is expressed as a function of $f_{l,\text{rup}}/f_{c0}$, corresponding to $\varepsilon_{h,\text{rup}}$, by

$$\Delta_c = A_0\left(\frac{f_{l,\text{rup}}}{f_{c0}}\right)^{A_1} \tag{5}$$

where A_0 and A_1 represent the regression coefficients. Hence, putting Eq. (5) in Eq. (4) yields

$$\frac{f_{cc}}{f_{c0}} = 1 + A_0\left(\frac{f_{l,\text{rup}}}{f_{c0}}\right)^{A_1} \tag{6}$$

Replacing Eq. (2) in Eq. (6) leads to

$$\frac{f_{cc}}{f_{c0}} = 1 + A_0\left(\frac{K_L\varepsilon_{h,\text{rup}}}{f_{c0}}\right)^{A_1} = 1 + A_0(\psi)^{A_1}\left(\frac{K_L}{f_{c0}}\varepsilon_{fu}\right)^{A_1} \tag{7}$$

To establish a regression analysis-based developed predictive formulation for f_{cc}/f_{c0} as a function of the key variables of K_L, f_{c0}, and ε_{fu}, Eq. (7) was restructured as

$$\frac{f_{cc}}{f_{c0}} = 1 + A_2(K_L)^{A_3}(f_{c0})^{A_4}(\varepsilon_{fu})^{A_5} \tag{8}$$

where A_2, A_3, A_4, and A_5 are the regression coefficients. Using the regression analysis technique implemented on 1,517 experimental data, these coefficients were obtained: $A_2 = 3.2\beta_0$, $\beta_0 = f_{c0}/15 \le 1$, $A_3 = 0.93$, $A_4 = -1.28$ and $A_5 = 0.69$. Thus, Eq. (8) can be written as

$$\frac{f_{cc}}{f_{c0}} = 1 + 3.2\beta_0 K_L^{0.91} f_{c0}^{-1.32}\varepsilon_{fu}^{0.67} \tag{9a}$$

$$\frac{f_{cc}}{f_{c0}} = 1 + 4.14\frac{K_L^{0.24}}{f_{c0}^{0.65}/\beta_0}\left(\frac{f_{l,\text{rup}}}{f_{c0}}\right)^{0.67} \tag{9b}$$

where by rearranging Eq. (9*a*), f_{cc}/f_{c0} can be determined as a function of $f_{l,\text{rup}}/f_{c0}$, by assuming $\varepsilon_{h,\text{rup}} = 0.68\varepsilon_{fu}$ (Baji et al. 2016), as shown in Eq. (9*a*). As can be seen, the magnitude of the change of f_{cc}/f_{c0} with $f_{l,\text{rup}}/f_{c0}$ is significantly dependent on concrete strength (f_{c0}) and FRP confinement stiffness (K_L). Experimental studies (Ozbakkaloglu and Akin 2012; Vincent and Ozbakkaloglu 2013) evidenced the significant degree of dominance of concrete strength class (low-, normal-, high-, and ultrahigh-strength concrete) in the effectiveness of the FRP confinement system (f_{cc}/f_{c0}). It was found that at a certain level of $f_{l,\text{rup}}/f_{c0}$, f_{cc}/f_{c0} decreases with increasing f_{c0}, which is in agreement with the proposed model of Eq. (9*b*). It should be noted that $\beta_0 = f_{c0}/15 \le 1$ is the term considered to modify the effect of f_{c0} on f_{cc}/f_{c0} for low-strength concrete specimens with FRP confinement. Fig. 3(a) demonstrates the relation of $Y_{fc} = (f_{cc}^{\text{Exp}}/f_{c0} - 1)/(3.2K_L^{0.91}\varepsilon_{fu}^{0.67})$ [obtained by rearranging Eq. (9*a*)] with f_{c0} based on the data from low-strength concrete specimens included in the database. As can be seen, considering that the best-fit relation of Y_{fc} and f_{c0} was obtained as $Y_{fc} = f_{c0}^{-1.32}$ based on regression analysis using a single power function, the model would lead to overestimation of the experimental counterparts. However, by considering the term of β_0, the model could present a better predictive performance for f_{cc} of very low-strength concrete specimens. In Fig. 3(b), the correlation of Eq. (9) with f_{c0} for a large range of 6.6 MPa $\le f_{c0} \le$ 204 MPa is evaluated. The results demonstrate that the variables of $f_{cc}^{\text{Ana}}/f_{cc}^{\text{Exp}}$ and f_{c0} are almost uncorrelated. Therefore, the proposed model could provide uniform predictions with respect to f_{c0}, representing successful simulation of the concrete strength effect in f_{cc}/f_{c0}.

Since the developed equation was derived based on Eq. (6) (f_{cc}/f_{c0} and $f_{l,\text{rup}}/f_{c0}$ relation), the effect of column dimension size was not considered in its development. To assess the dominance degree of the size effect on the model's performance, the error distribution of Eq. (9*a*) (the ratio of analytical and experimental predictions as $(\Delta_c)^{\text{Ana}}/(\Delta_c)^{\text{Exp}}$) with the normalized column dimension size (b/150) is shown in Fig. 3(c). Despite the larger scattering of results, they reveal a tendency for Eq. (9*a*) to slightly underestimate and then overestimate from small to large-sized test specimens of FFCC. By introducing β_{SE} as the best-fit relationship of $(\Delta_c)^{\text{Ana}}/(\Delta_c)^{\text{Exp}}$ and b/150, this parameter was obtained from regression analysis performed on 1,517 experimental data:

$$\beta_{\text{SE}} = \frac{(\Delta_c)^{\text{Ana}}}{(\Delta_c)^{\text{Exp}}} = \left(\frac{b}{150}\right)^{0.2} \le 1.1 \tag{10}$$

where $\beta_{\text{SE}} = 1$ for FFCC having $b = 150$ mm. Henceforth, $(\Delta_c)^{\text{Exp}}$ can be estimated as $(\Delta_c)^{\text{Ana}}/\beta_{\text{SE}}$, in which $(\Delta_c)^{\text{Ana}} = 3.2\beta_0 K_L^{0.91} f_{c0}^{-1.32}\varepsilon_{fu}^{0.67}$. Consequently, Eq. (9*a*) can be rearranged, considering the column dimension size effect, as

$$\frac{f_{cc}}{f_{c0}} = 1 + (\Delta_c)^{\text{Exp}} \simeq 1 + \frac{(\Delta_c)^{\text{Ana}}}{\beta_{\text{SE}}} = 1 + \frac{3.2}{\beta_{\text{SE}}}\beta_0 K_L^{0.91} f_{c0}^{-1.32}\varepsilon_{fu}^{0.67} \tag{11}$$

Fig. 3(d) evaluates the predictive performance of the developed model [Eq. (11)] for predicting f_{cc} of FFCC. As can be seen, the proposed model is able to predict the experimental counterparts with sufficient accuracy based on the attained statistical indicators [mean value (MV), coefficient of variation (CoV), mean absolute

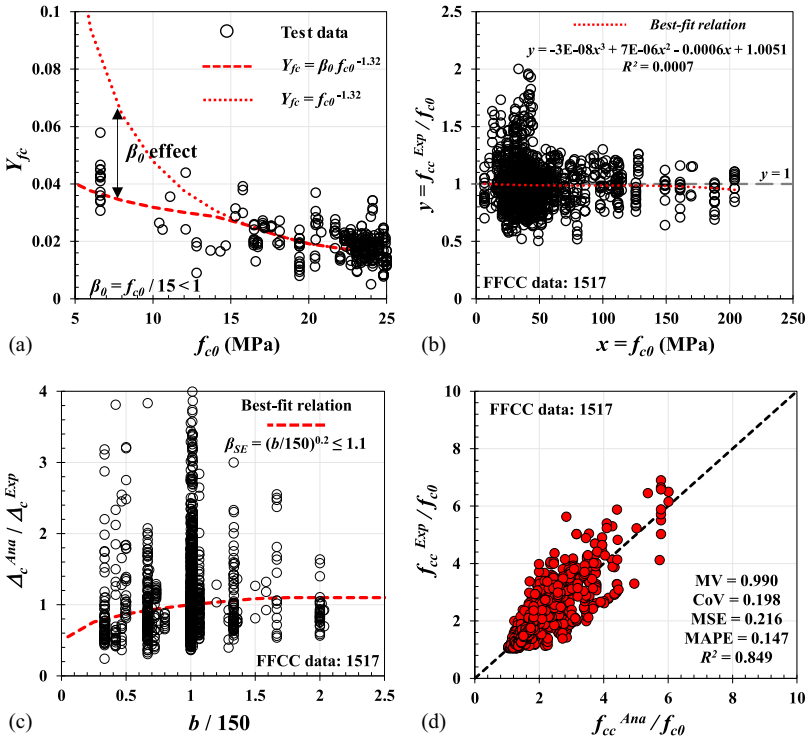

Fig. 3. (a) Variation of Y_{fc} with f_{c0}; (b) predictive performance of Eq. (9); (c) variation of error distribution with b/150; and (d) predictive performance of Eq. (11). MV = mean value; CoV = coefficient of variation; MSE = mean squared error; MAPE = mean absolute percentage error.

percentage error (MAPE), mean squared error (MSE), and R squared (R^2)].

For a further examination of the developed model capability, Table 4 compares its prediction capability with that of the considered existing models (presented in Table 3). It can be seen that although the models suggested by *fib* (2019) and ACI 440.2R-17 (ACI 2017) presented the best estimation capability of the existing ones considered, the proposed formulation showed a better prediction of f_{cc}.

FFSC Column Elements

For the case of FFSC, the experimental evidence reported by Shan et al. (2019) demonstrated that the FRP confinement-induced enhancement, in terms of compressive strength, is strongly dependent on the sectional corner radius ratio ($R_r = 2r/b$). Accordingly, from the case with $R_r = 1$ (FFCC) to that of $R_r = 0$ (FFSC with sharp edges), the compressive strength of FFSC is reduced significantly.

To evaluate the dominance degree of R_r on confinement-induced enhancements, the predictive performance of Eq. (11) (exclusively developed for FFCC with no consideration of the noncircularity effect) was analyzed for FFSC specimens with different levels of R_r. As demonstrated in Fig. 4(a), Eq. (11) leads to significant overestimation, predominantly for FFSC cases with a low value of R_r. Accordingly, to consider the noncircularity effect, a model parameter (β_R) was defined as the best-fit relationship of $(\Delta_c)^{Ana}/(\Delta_c)^{Exp}$ (where $(\Delta_c)^{Ana} = 3.2\beta_0 K_L^{0.91} f_{c0}^{-1.32} \varepsilon_{fu}^{0.67}/\beta_{SE}$) with R_r. Based on the regression analysis technique implemented on 256 test results of FFSC, β_R was derived as:

$$\beta_R = \frac{(\Delta_c)^{Ana}}{(\Delta_c)^{Exp}} = 0.85 R_r^{-0.75} \ge 1 \tag{12}$$

where $\beta_R = 1$ for FFCC with $R_r = 1$. Accordingly, to simulate the noncircularity effect, considering that $(\Delta_c)^{Exp}$ can be estimated as $(\Delta_c)^{Ana}/\beta_R$, Eq. (11) can be rearranged as

$$\frac{f_{cc}}{f_{c0}} = 1 + (\Delta_c)^{Exp} \simeq 1 + \frac{(\Delta_c)^{Ana}}{\beta_R} = 1 + \frac{3.2}{\beta_{SE}\beta_R} \beta_0 K_L^{0.91} f_{c0}^{-1.32} \varepsilon_{fu}^{0.67} \tag{13}$$

In Fig. 4(b), the close agreement of analytical and experimental results verifies the reliable performance of the proposed formulation [Eq. (13)].

Additionally, in Table 5, the predictive performance of Eq. (13) is compared with that of the considered existing predictive models (Table 3). As shown, the proposed model and those developed by

Table 4. Statistical assessment of predictive performance of considered and proposed models for f_{cc} of FFCC

ID	Type	Test data	MV	CoV	MAPE	MSE	R^2
Proposed model	FFCC	1,517	0.990	0.198	0.147	0.216	0.849
fib (2019)			0.902	0.226	0.183	0.336	0.812
CNR DT 200/2004 (CNR 2004)			0.770	0.259	0.262	0.759	0.795
Guo et al. (2018, 2019)			0.760	0.252	0.272	0.666	0.816
ACI 440.2R-17 (ACI 2017)			0.948	0.273	0.188	0.366	0.806
Wei and Wu (2012)			1.089	0.276	0.194	0.426	0.807
Cao et al. (2016)			1.145	0.300	0.213	0.951	0.756

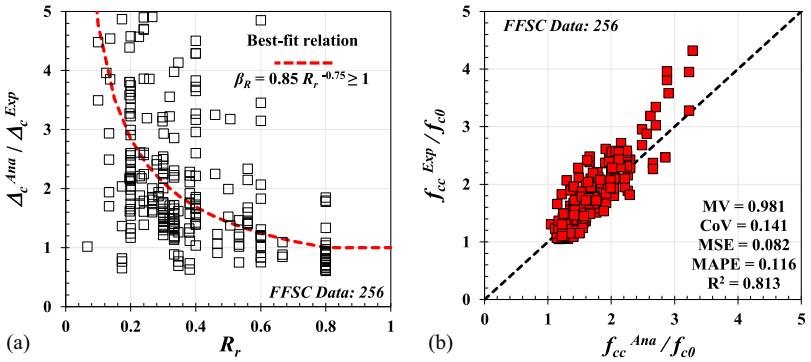

Fig. 4. (a) Variation of error distribution with R_r; and (b) predictive performance of Eq. (13).

Wei and Wu (2012) and Cao et al. (2016) attained almost similar results of statistical indicators, which are the best compared with those obtained from the other models.

FFRC Column Elements

For the case of FFRC, it was evidenced by Ozbakkaloglu (2013) that increasing the sectional aspect ratio ($R_{ca} = h/b$) brings about a remarkable reduction in the confinement effectiveness in terms of axial compressive strength. To assess the dominance degree of R_{ca} on confinement-induced enhancements, the predictive performance of Eq. (13) (exclusively developed for FFCC or FFSC with no consideration of the sectional aspect ratio effect) was analyzed for FFRC specimens with different levels of R_{ca}. Fig. 5(a) reveals that, using Eq. (13), significant overestimates in the axial compressive strength of FFRC are obtained, predominantly for FFRC with a high value of R_{ca}. Consequently, to consider the effect of R_{ca}, a model parameter β_λ was defined as the best-fit relationship between the error index $(\Delta_c)^{Ana}/(\Delta_c)^{Exp}$ [where $(\Delta_c)^{Ana} = 3.2\beta_0 K_L^{0.91} f_{c0}^{-1.32} \varepsilon_{fu}^{0.67} / \beta_{SE}\beta_R$] and R_{ca}. Based on regression analysis performed on 145 experimental data of FFSC, β_λ was derived as

$$\beta_\lambda = \frac{(\Delta_c)^{Ana}}{(\Delta_c)^{Exp}} = R_{ca}^{2.2} \leq 4 \tag{14}$$

where $\beta_\lambda = 1$ for FFCC and FFSC having $R_{ca} = 1$. Considering $(\Delta_c)^{Exp} = (\Delta_c)^{Ana}/\beta_\lambda$, Eq. (13) can be rearranged considering the sectional aspect ratio effect:

$$\frac{f_{cc}}{f_{c0}} = 1 + (\Delta_c)^{Exp} \simeq 1 + \frac{(\Delta_c)^{Ana}}{\beta_\lambda} = 1 + \frac{3.2}{\beta_{SE}\beta_R\beta_\lambda}\beta_0 K_L^{0.91} f_{c0}^{-1.32} \varepsilon_{fu}^{0.67} \tag{15}$$

Fig. 5(b) evidences the predictive performance of the developed model for the case of FFRC, with a unified character with FFCC or FFSC, based on the obtained statistical indicators.

Furthermore, Table 6 compares the performance of Eq. (15) and the available considered models in the prediction of f_{cc} of FFRC. As can be seen, the proposed model and Cao et al. (2016) showed the best predictive performance with almost similar achieved statistical indicators.

FPCC, FPSC, or FPRC Column Elements

Experimental studies conducted by Zeng et al. (2017, 2018) demonstrated that the effectiveness of the partial confinement system is mainly dependent on the influential factor of s_f (the distance between FRP strips). Shayanfar et al. (2021a, 2022a) revealed that by increasing s_f from zero ($s_f = 0$, representing fully confined concrete) to above L_{d0} (where $s_f \geq L_{d0}$ defines the damage zone length of unconfined concrete), the effectiveness of FRP partial confinement on axial strength becomes quite insignificant, and can reasonably be neglected.

To assess the influence of the confining system type in terms of confinement-induced improvements, 199 test specimens of FPCC, FPSC, or FPRC collected in the database were simulated by Eq. (15) (developed exclusively for full confinement arrangement), and the results are presented in Fig. 6(a). It is noteworthy that, since the confinement stiffness of FRP partial system is a function of s_f and the width of the FRP strip (w_f), the term of K_L in Eq. (15) needs to be modified, as

$$K_L = 2\frac{n_f^\kappa t_f E_f}{b}\left(\frac{w_f}{w_f + s_f}\right) \tag{16}$$

In fact, the term $w_f/(w_f + s_f)$ specifically represents the unification in terms of FRP volumetric ratio for PC concrete (Wu and Wei 2016; Shayanfar et al. 2020), where, owing to its unified character, Eq. (16) results in the same prediction as Eq. (3) presented for full confinement arrangement ($s_f = 0$). As shown in Fig. 6(a), by increasing the normalized distance between FRP strips ($R_{sf} = s_f/b$), Eq. (15) overestimated the experimental counterparts, particularly beyond $R_{sf} = 0.25$. Consequently, a model parameter (β_P), addressing the effect of partially imposed confinement, was defined as the

Table 5. Statistical assessment of predictive performance of considered and proposed models for f_{cc} of FFSC

ID	Type	Test data	MV	CoV	MAPE	MSE	R^2
Proposed model	FFSC	256	0.981	0.141	0.116	0.082	0.813
fib (2019)			0.886	0.176	0.156	0.183	0.770
CNR DT 200/2004 (CNR 2004)			0.854	0.251	0.210	0.353	0.549
Guo et al. (2018, 2019)			0.758	0.225	0.257	0.454	0.583
ACI 440.2R-17 (ACI 2017)			0.898	0.208	0.167	0.188	0.662
Wei and Wu (2012)			0.984	0.161	0.123	0.104	0.786
Cao et al. (2016)			1.003	0.152	0.119	0.082	0.804

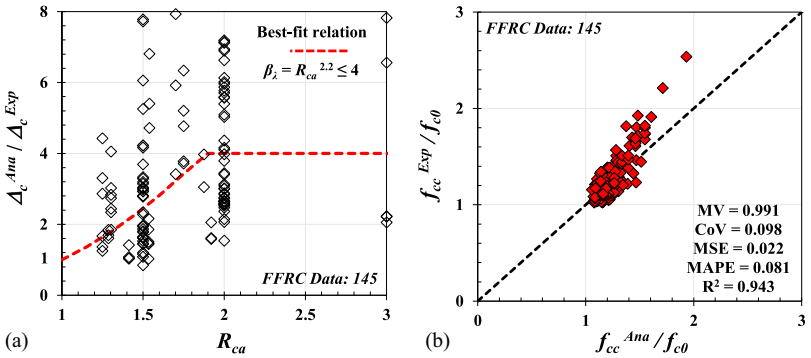

Fig. 5. (a) Variation of error distribution with R_{ca}; and (b) predictive performance of Eq. (15).

Table 6. Statistical assessment of predictive performance of considered and proposed models for f_{cc} of FFRC

ID	Type	Test data	MV	CoV	MAPE	MSE	R^2
Proposed model	FFRC	145	0.991	0.098	0.081	0.022	0.943
fib (2019)			1.026	0.158	0.136	0.040	0.873
CNR DT 200/2004 (CNR 2004)			1.031	0.178	0.155	0.058	0.827
Guo et al. (2018, 2019)			1.332	0.265	0.354	0.372	0.693
ACI 440.2R-17 (ACI 2017)			1.053	0.147	0.132	0.040	0.852
Wei and Wu (2012)			1.128	0.125	0.149	0.049	0.909
Cao et al. (2016)			1.019	0.105	0.092	0.022	0.938

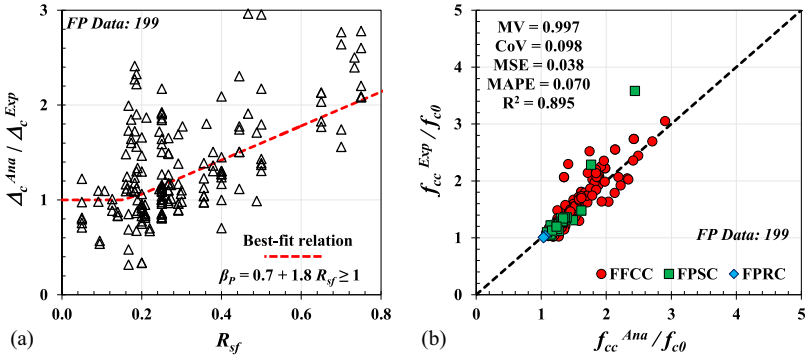

Fig. 6. (a) Variation of error distribution with R_{sf}; and (b) predictive performance of Eq. (18).

best-fit relationship between $(\Delta_c)^{Ana}/(\Delta_c)^{Exp}$ [where $(\Delta_c)^{Ana} = 3.2\beta_0 K_L^{0.91} f_{c0}^{-1.32} \varepsilon_{fu}^{0.67} \beta_{SE} \beta_R \beta_\lambda$] and R_{sf}, obtained from regression analysis:

$$\beta_P = \frac{(\Delta_c)^{Ana}}{(\Delta_c)^{Exp}} = 0.7 + 1.8R_{sf} \ge 1 \tag{17}$$

where $\beta_P = 1$ for FFCC, FFSC, or FFRC having $R_{sf} = 0$. Considering $(\Delta_c)^{Exp} = (\Delta_c)^{Ana}/\beta_P$, Eq. (15) can be rearranged considering the sectional aspect ratio effect, as

$$\frac{f_{cc}}{f_{c0}} = 1 + (\Delta_c)^{Exp} \simeq 1 + \frac{(\Delta_c)^{Ana}}{\beta_P} = 1 + \frac{3.2}{\beta_{SE}\beta_R\beta_\lambda\beta_P} \beta_0 K_L^{0.91} f_{c0}^{-1.32} \varepsilon_{fu}^{0.67} \tag{18}$$

The predictive performance of the developed model for cases with partial confinement configuration is demonstrated in Fig. 6(b). As evidenced by the obtained statistical indicators, Eq. (18) provided excellent agreement with the experimental counterparts, confirming the reliability of the model parameter β_P.

Moreover Table 7 compares the predictive performances of Eq. (18) and of the models suggested by CNR DT 200/2004 (CNR 2004), Guo et al. (2018, 2019), and fib (2019). It can be seen that even though the model suggested by CNR DT 200/2004 (CNR 2004) resulted in the best predictions among the existing models, the proposed formulation presented a better prediction of f_{cc} for FPCC, FPSC, or FPRC.

Determination of μ_ε of FRP-Confined Concrete Columns

This section provides the determination of strain ductility (μ_ε) of FRP-confined concrete based on regression analysis performed on 2,050 test data collected in the database (Table 2). Firstly, a new theoretical-based model for calculating μ_ε, based on Poisson's ratio effect (the ratio between FRP hoop strain and axial strain) is derived. Then, this model is restructured to have a proper format for application of the regression analysis technique. For FFCC, the model is calibrated using 1,462 experimental results, where the size effect is considered. The strain ductility model is then extended to be applicable to noncircular columns with full confinement (FFSC and FFRC) by introducing the influence of the

Table 7. Statistical assessment of predictive performance of considered and proposed models for f_{cc} of FPCC, FPSC, and FPRC

ID	Type	Test data	MV	CoV	MAPE	MSE	R^2
Proposed model	FPCC, FPSC, FPRC	199	0.997	0.098	0.070	0.038	0.895
fib (2019)			1.108	0.162	0.160	0.099	0.797
CNR DT 200/2004 (CNR 2004)			0.951	0.174	0.143	0.075	0.816
Guo et al. (2018, 2019)			0.936	0.163	0.118	0.104	0.798

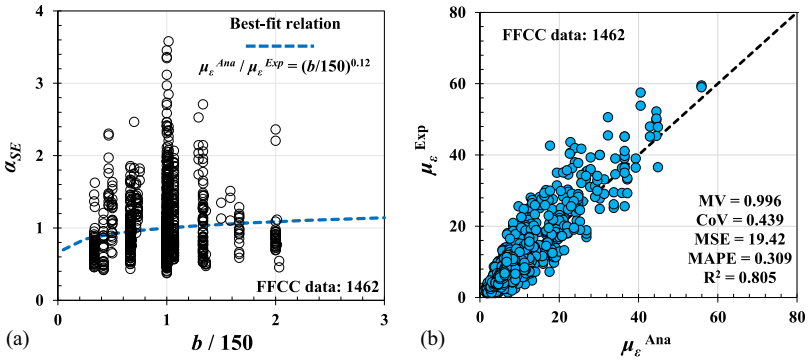

Fig. 7. (a) Relation of $\mu_\varepsilon^{\text{Ana}}/\mu_\varepsilon^{\text{Exp}}$ versus b/150; and (b) predictive performance of Eq. (25).

noncircularity effect and sectional aspect ratio on the column ductility, which is calibrated using 404 experimental results of FFSC and FFRC. Finally, the developed model is extended for concrete columns with a partial confining system by considering the influence of the partially imposed confinement in terms of μ_ε, calibrated based on 206 experimental results of FPCC, FPSC, and FPRC.

FFCC Column Elements

The ultimate axial strain (ε_{cu}) of FRP-confined circular concrete columns under compression can be defined when the hoop strain in FRP jacket reaches $\varepsilon_{h,\text{rup}}$. Based on the Poisson's ratio effect concept, the secant Poisson's ratio (ν_u) at the rupture stage can be approximated as the ratio of $\varepsilon_{h,\text{rup}}$ and ε_{cu}. Accordingly, ε_{cu} is obtained as a main function of $\varepsilon_{h,\text{rup}}$ and ν_u:

$$\varepsilon_{cu} = \frac{\varepsilon_{h,\text{rup}}}{\nu_u} \tag{19}$$

Considering $\varepsilon_{h,\text{rup}} = \psi\varepsilon_{fu}$, where ψ is a constant value, Eq. (19) can be expressed as

$$\varepsilon_{cu} = \frac{\psi\varepsilon_{fu}}{\nu_u} \tag{20}$$

By dividing both sides of Eq. (20) by ε_{c0} (the axial strain corresponding to f_{c0}), μ_ε can be derived as

$$\mu_\varepsilon = \frac{\varepsilon_{cu}}{\varepsilon_{c0}} = \frac{\psi\varepsilon_{fu}}{\nu_u\varepsilon_{c0}} \tag{21}$$

The studies conducted by Mirmiran and Shahawy (1997), Baji et al. (2016), and Shayanfar et al. (2020, 2021b, 2022c) evidenced that ν_u is strongly dependent on K_L and f_{c0}. Furthermore, Lim and Ozbakkaloglu (2014) and Shayanfar et al. (2023b) demonstrated that ε_{c0} is also a main function of f_{c0}. Hence, for the establishment of a proper basis for regression analysis, Eq. (21) is restructured as

$$\mu_\varepsilon = B_0 K_L^{B_1} f_{c0}^{B_2} \varepsilon_{fu}^{B_3} \tag{22}$$

where B_0, B_1, B_2, and B_3 are the regression coefficients, determined as $B_0 = 300$, $B_1 = 0.56$, $B_2 = -0.78$, and $B_3 = 1.17$, obtained from regression analysis, resulting in

$$\mu_\varepsilon = 300 K_L^{0.56} f_{c0}^{-0.78} \varepsilon_{fu}^{1.17} \tag{23}$$

It is noteworthy that, since the developed equation was derived based on Eq. (21), the influence of column dimension size on μ_ε was not considered. To evaluate the degree of the dominance of the column dimension size on the model's performance, Fig. 7(a) analyzes the error distribution of Eq. (23) (the ratio of the results obtained analytically to the results obtained experimentally, $(\mu_\varepsilon)^{\text{Ana}}/(\mu_\varepsilon)^{\text{Exp}}$) with b/150. It can be seen that for small-sized test specimens of FFCC, conservative results were obtained. Accordingly, using the regression analysis technique implemented on 1,462 experimental results of FFCC, the relationship of $(\mu_\varepsilon)^{\text{Ana}}/(\mu_\varepsilon)^{\text{Exp}}$ with b/150 was derived, resulting in

$$\alpha_{\text{SE}} = \frac{(\mu_\varepsilon)^{\text{Ana}}}{(\mu_\varepsilon)^{\text{Exp}}} \simeq \left(\frac{b}{150}\right)^{0.12} \leq 1 \tag{24}$$

where $\alpha_{\text{SE}} = 1$ for FFCC with $b = 150$ mm. Therefore, Eq. (23) can be updated by considering the column dimension:

$$\mu_\varepsilon = \frac{300}{\alpha_{\text{SE}}} K_L^{0.56} f_{c0}^{-0.78} \varepsilon_{fu}^{1.17} \tag{25}$$

The performance of Eq. (25) is demonstrated in Fig. 7(b). The obtained statistical indicators verify that there is a good agreement between the analytical and experimental results.

For a further examination of the capability of the proposed model, Table 8 compares the predictive performances of Eq. (25) and the considered ductility models. As can be seen, although the models recommended by fib (2019) and Guo et al. (2018, 2019) presented the best performance of the existing models, Eq. (25) showed by far a superior performance in the prediction of μ_ε.

It is noteworthy that the fundamental assumption in the considered ductility models, as presented in Eq. (1) ($\mu_\varepsilon = k_0 + \Psi_c$), is that FRP confinement-induced improvement in μ_ε is simulated by using the Ψ_c term, where for the case of unconfined concrete ($\Psi_c = 0$), therefore, $\mu_\varepsilon = k_0$. Nevertheless, in this study, the framework of Eq. (22) ($\mu_\varepsilon = \Psi_c$), derived based on Poisson's ratio effect [Eq. (21)], was adopted for the statistical modeling of μ_ε. The preliminary comparative assessment of the framework of Eq. (1) with

Table 8. Statistical assessment of predictive performance of considered and proposed models for μ_ε of FFCC

ID	Type	Test data	MV	CoV	MAPE	MSE	R^2
Proposed model	FFCC	1,462	0.996	0.439	0.309	19.42	0.805
fib (2019)			0.910	0.486	0.339	32.57	0.689
CNR DT 200/2004 (CNR 2004)			0.664	0.598	0.447	98.00	0.417
Guo et al. (2018, 2019)			0.999	0.493	0.343	25.25	0.727
ACI 440.2R-17 (ACI 2017)			1.036	0.549	0.370	37.04	0.603
Wei and Wu (2012)			1.053	0.560	0.393	61.51	0.339
Cao et al. (2016)			1.371	0.507	0.500	75.01	0.564

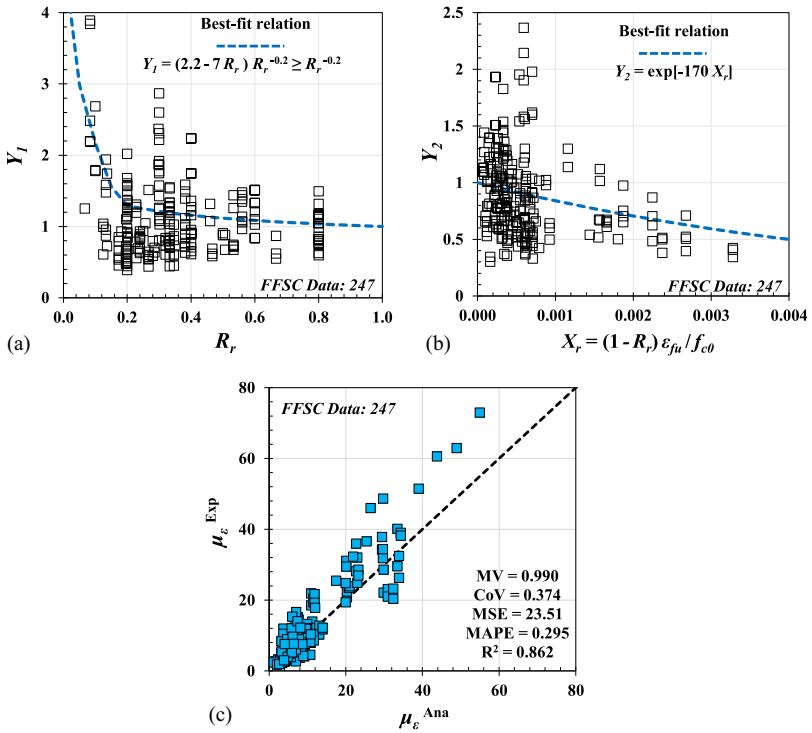

Fig. 8. (a) Relation of $\mu_\varepsilon^{Ana}/\mu_\varepsilon^{Exp}$ versus R_r; (b) relation of $\mu_\varepsilon^{Ana}/\mu_\varepsilon^{Exp}$ versus X_r; and (c) predictive performance of Eq. (30).

the proposed framework of Eq. (22) demonstrated that more accurate predictive formulation can be developed by regression analysis by adopting the framework of Eq. (22) rather than that of Eq. (1).

FFSC Column Elements

To assess the influence of the noncircularity effect on μ_ε, the performance of Eq. (25) (developed exclusively for FFCC) was analyzed for predicting μ_ε of FFSC with different levels of R_r. Fig. 8(a) demonstrates the distribution of Eq. (25)'s error index of $Y_1 = (\mu_\varepsilon)^{Ana}/(\mu_\varepsilon)^{Exp}$ with R_r. It is evident that there are nonconservative results, particularly for FFSC with a low value of R_r. Based on regression analysis performed on 247 experimental results of FFSC, the best-fit relation of Y_1 and R_r was obtained, resulting in

$$Y_1 = (2.2 - 7R_r)R_r^{-0.2} \geq R_r^{-0.2} \tag{26}$$

Thus, introducing Eq. (26) into Eq. (25) yields:

$$\mu_\varepsilon = \frac{300}{Y_1 \alpha_{SE}} K_L^{0.56} f_{c0}^{-0.78} \varepsilon_{fu}^{1.17} \tag{27}$$

For further examination of the performance of the developed model, the distribution of Eq. (27)'s error index of $Y_2 = (\mu_\varepsilon)^{Ana}/(\mu_\varepsilon)^{Exp}$ as a function of $X_r = (1 - R_b)\varepsilon_{fu}/f_{c0}$ (where $X_r = 0$ and $X_r > 0$ for FFCC and FFSC, respectively) is demonstrated in Fig. 8(b). The aim is to consider X_r the integrated influence of R_b, the ultimate tensile strain of FRP, and the compressive strength of unconfined concrete on μ_ε. As shown, by increasing X_r, Y_2 is reduced noticeably. The best-fit relation of Y_2 and X_r was obtained from regression analysis, resulting in

$$Y_2 = e^{-170X_r} \tag{28}$$

Hence, to consider the influence of X_r on μ_ε, Eq. (27) can be reorganized using Eq. (28):

$$\mu_\varepsilon = \frac{300}{Y_1 Y_2 \alpha_{SE}} K_L^{0.56} f_{c0}^{-0.78} \varepsilon_{fu}^{1.17} \tag{29}$$

As a result, by rearranging this equation, considering the noncircularity effect, μ_ε can be determined from

$$\mu_\varepsilon = \frac{300}{\alpha_{SE}\alpha_R} K_L^{0.56} f_{c0}^{-0.78} \varepsilon_{fu}^{1.17} \tag{30}$$

in which

$$\alpha_R = Y_1 Y_2 = (2.2 - 7R_r)\frac{e^{-170X_r}}{R_r^{0.2}} \geq \frac{e^{-170X_r}}{R_r^{0.2}} \tag{31}$$

where $\alpha_R = 1$ for FFCC. Fig. 8(c) examines the predictive performance of Eq. (30). As shown, there is a good agreement between the experimental results and those obtained from Eq. (30).

Furthermore, Table 9 compares the performance of Eq. (30) with that provided by the considered models in the prediction of μ_ε of FFSC. It can be seen that, based on achieved statistical indicators, the proposed model showed the best predictive performance of all the models.

FFRC Column Elements

For the case of FFRC, the performance of Eq. (30) (developed exclusively for FFCC or FFSC) was analyzed to evaluate the dominance degree of sectional aspect ratio ($R_{ca} = h/b$) on μ_ε, as shown in Fig. 9(a). Consequently, the best-fit relation of α_λ [Eq. (30)'s error index, $\alpha_\lambda = (\mu_\varepsilon)^{\text{Ana}}/(\mu_\varepsilon)^{\text{Exp}}$] as a function of R_{ca} was derived based on regression analysis performed on 157 test data of FFRC, resulting in

$$\alpha_\lambda = 0.84R_{ca}^{0.3} \geq 1 \tag{32}$$

where $\alpha_\lambda = 1$ for $R_{ca} < 1.8$. Therefore, by introducing Eq. (32) into Eq. (30), μ_ε of FFRC can be predicted with a unified character to FFCC and FFSC, with

$$\mu_\varepsilon = \frac{300}{\alpha_{\text{SE}}\alpha_R\alpha_\lambda} K_L^{0.56} f_{c0}^{-0.78} \varepsilon_{fu}^{1.17} \tag{33}$$

The predictive performance of Eq. (33) is evaluated in Fig. 9(b). As can be seen, despite the obtained conservative results for some specimens with $(\mu_\varepsilon)^{\text{Exp}} > 20$, the developed model is capable of efficiently predicting the experimental counterparts of FFRC based on the obtained statistical indicators. Furthermore, in Table 10, the performance of Eq. (33) is compared with that of the considered models in the prediction of μ_ε of FFRC. It can be seen that, although the model suggested by Cao et al. (2016) exhibited the best performance among the existing models, the proposed model led to a better prediction of μ_ε.

FPCC, FPSC, or FPRC Column Elements

To assess the influence of partially confining systems in terms of μ_ε, Eq. (33), developed exclusively for cases with full confinement, was applied to 184 test specimens of FPCC, FPSC, and FPRC. Fig. 10(a) demonstrates the distribution of Eq. (33)'s error index of $Y_3 = (\mu_\varepsilon)^{\text{Ana}}/(\mu_\varepsilon)^{\text{Exp}}$ with R_{sf}, where the best-fit relation between them was obtained as

$$Y_3 = 1 - 1.42R_{sf} + 7R_{sf}^2 - 7R_{sf}^3 \tag{34}$$

where this equation is applicable to $R_{sf} \leq 0.75$. Subsequently, by considering the effects of concrete strength (f_{c0}) and column aspect ratio (L/b) as other influential variables on μ_ε, a model parameter (α_P) was defined based on regression analysis for partially imposed confinement strategy, as

$$\alpha_P = \xi Y_3 = \xi(1 - 1.42R_{sf} + 7R_{sf}^2 - 7R_{sf}^3) \tag{35}$$

in which

$$\xi = 1 + (\xi_0 - 1)\frac{R_{sf}}{0.15} \text{ for } R_{sf} \leq 0.15 \tag{36a}$$

$$\xi = \xi_0 \text{ for } R_{sf} \geq 0.15 \tag{36b}$$

$$\xi_0 = 0.125 f_{c0}^{0.12}\left(\frac{L}{b}\right)^{1.7} \leq 1.5 \tag{37}$$

where $\xi = 1$ and $\alpha_P = 1$ are adopted for FFCC, FFSC, or FFRC with $R_{sf} = 0$. Thus, by replacing Eq. (35) in Eq. (33), for the specimens with partial confinement arrangement, μ_ε can be determined from

$$\mu_\varepsilon = \frac{300}{\alpha_{\text{SE}}\alpha_R\alpha_\lambda\alpha_P} K_L^{0.56} f_{c0}^{-0.78} \varepsilon_{fu}^{1.17} \tag{38}$$

In Fig. 10(b), the predictions from Eq. (38) are compared with those reported by test data, and a good agreement between them can be observed.

Moreover, Table 11 compares the performance of Eq. (38) with that provided by the CNR DT 200/2004 (CNR 2004), Guo et al. (2018, 2019), and *fib* (2019) models. It can be seen that even though *fib* (2019) showed the best performance among the considered models, a considerably better prediction of μ_ε for the FPCC, FPSC, and FPRC specimens is obtained from the unified proposed model based on Eq. (38).

Unified Compressive Strength and Strain Ductility Models

In this section, the predictive performance of the developed models for the calculation of f_{cc} and μ_ε of FRP-confined concrete columns under axial compressive loading is assessed. By rearranging Eq. (18), the unified strength model to predict f_{cc} of various cases of FRP-confined concrete columns is proposed as

$$\frac{f_{cu}}{f_{c0}} = 1 + \frac{3.2}{\beta_{\text{UF}}}\beta_0 K_L^{0.91} f_{c0}^{-1.32} \varepsilon_{fu}^{0.67} \tag{39}$$

in which

$$\beta_{\text{UF}} = \beta_{\text{SE}}\beta_R\beta_\lambda\beta_P \tag{40}$$

where $\beta_{\text{UF}} = 1$ for FFCC. The model parameters of β_{SE}, β_R, β_λ, and β_P are calculated using Eqs. (10), (12), (14) and (17), respectively. Conversely, the unified strain ductility model to predict μ_ε can be

Table 9. Statistical assessment of predictive performance of considered and proposed models for μ_ε of FFSC

ID	Type	Test data	MV	CoV	MAPE	MSE	R^2
Proposed model	FFSC	247	0.990	0.374	0.295	23.51	0.862
fib (2019)			0.653	0.512	0.414	129.5	0.322
CNR DT 200/2004 (CNR 2004)			0.647	0.517	0.415	160.2	0.212
Guo et al. (2018, 2019)			0.768	0.479	0.366	96.21	0.660
ACI 440.2R-17 (ACI 2017)			0.720	0.510	0.390	112.8	0.483
Wei and Wu (2012)			1.061	0.513	0.416	113.0	0.179
Cao et al. (2016)			1.238	0.447	0.437	56.56	0.581

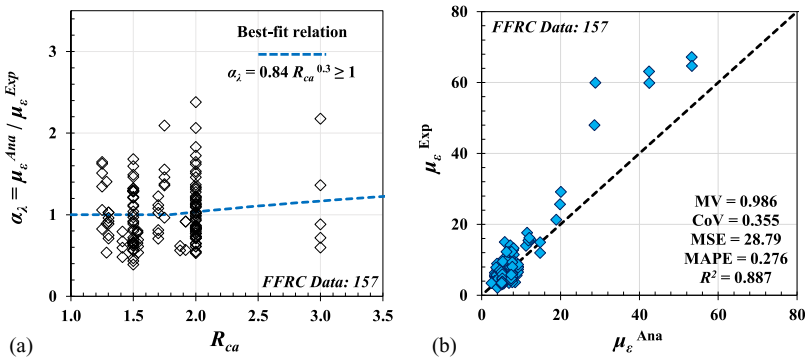

Fig. 9. (a) Relation of $\mu_\varepsilon^{\text{Ana}}/\mu_\varepsilon^{\text{Exp}}$ versus R_{ca}; and (b) predictive performance of Eq. (33).

Table 10. Statistical assessment of predictive performance of considered and proposed models for μ_ε of FFRC

ID	Type	Test data	MV	CoV	MAPE	MSE	R^2
Proposed model	FFRC	157	0.986	0.355	0.276	28.79	0.887
fib (2019)			0.665	0.413	0.364	130.1	0.259
CNR DT 200/2004 (CNR 2004)			0.609	0.379	0.405	153.0	0.156
Guo et al. (2018, 2019)			0.793	0.354	0.289	96.21	0.643
ACI 440.2R-17 (ACI 2017)			0.762	0.373	0.315	109.1	0.491
Wei and Wu (2012)			1.062	0.425	0.307	117.8	0.153
Cao et al. (2016)			1.024	0.376	0.276	80.96	0.607

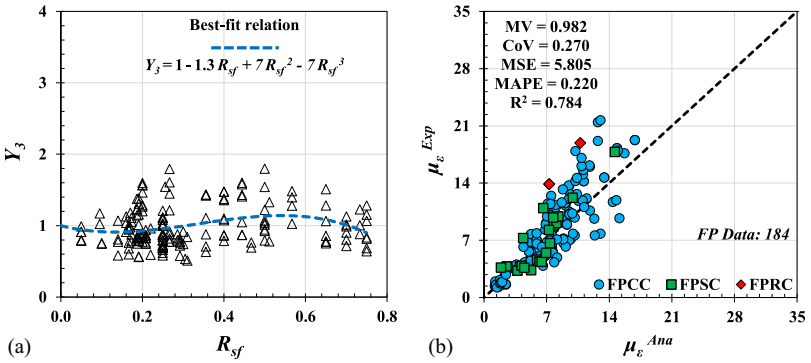

Fig. 10. (a) Relation of $\mu_\varepsilon^{\text{Ana}}/\mu_\varepsilon^{\text{Exp}}$ versus R_{sf}; and (b) predictive performance of Eq. (38).

derived by rearranging Eq. (38), as

$$\mu_\varepsilon = \frac{300}{\alpha_{\text{UF}}} K_L^{0.56} f_{c0}^{-0.78} \varepsilon_{fu}^{1.17} \tag{41}$$

in which

$$\alpha_{\text{UF}} = \alpha_{\text{SE}} \alpha_R \alpha_\lambda \alpha_P \tag{42}$$

where $\alpha_{\text{UF}} = 1$for FFCC, and α_{SE}, α_R, α_λ, and α_P are calculated using Eqs. (24), (31), (32) and (35), respectively.

Therefore, β_{UF} and α_{UF} can be considered as unification factors, not only for smooth transitions (prediction continuity) of the shapes of the columns' cross sections (from circular to square or rectangular), and the confining systems (from full to partial confinement), but also for considering the influences of cross-sectional shape and confining system in terms of f_{cc} and μ_ε. Furthermore, through this unification approach, uniform mathematical formulations were developed for all the confinement scenarios imposed on concrete columns (FFCC, FFSC, FFRC, FPCC, FPSC, and FPRC).

It should be noted that the proposed unification factors were developed or calibrated through implementation of the regression analysis technique. Accordingly, once more wide-ranging and larger datasets than those used in this study (Tables 1 and 2) are available, these factors can be recalibrated, resulting in a potential

Table 11. Statistical assessment of predictive performance of considered and proposed models for μ_ε of FPCC, FPSC, and FPRC

ID	Type	Test data	MV	CoV	MAPE	MSE	R^2
Proposed model	FPCC, FPSC, FPRC	184	0.982	0.270	0.220	5.805	0.784
fib (2019)			1.016	0.664	0.485	14.63	0.668
CNR DT 200/2004 (CNR 2004)			0.791	0.654	0.497	28.81	0.441
Guo et al. (2018, 2019)			1.103	0.696	0.525	14.89	0.644

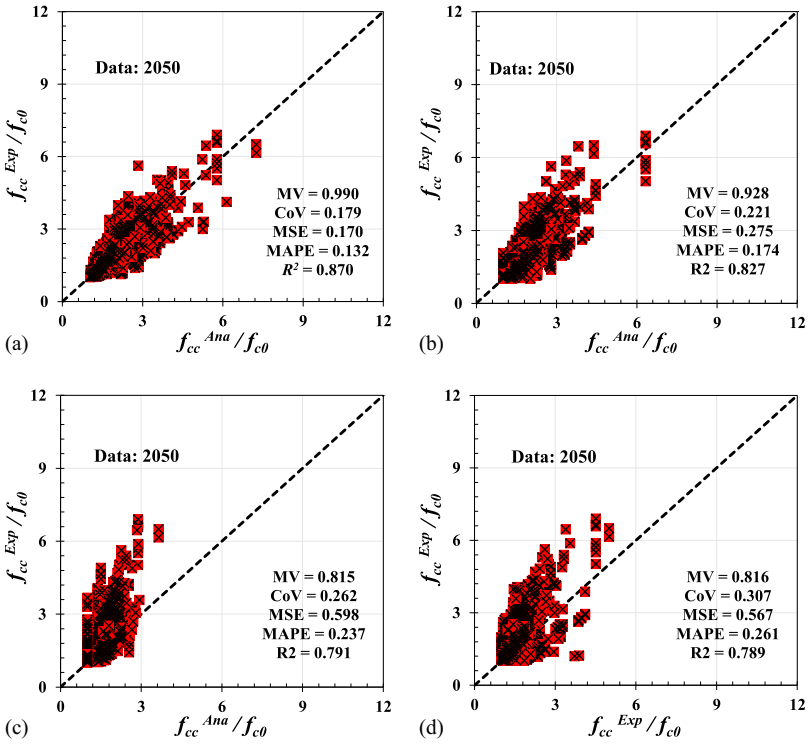

Fig. 11. Predictive performance of (a) proposed strength model; (b) *fib* (2019); (c) CNR DT 200/2004 (CNR 2004); and (d) Guo et al. (2018, 2019).

Table 12. Statistical assessment of available unified models for predicting f_{cc}

ID	Type	Test data	MV	CoV	MAPE	MSE	R^2
Proposed model	FF, FP	2,117	0.990	0.179	0.132	0.170	0.870
fib (2019)			0.928	0.221	0.174	0.275	0.827
CNR DT 200/2004 (CNR 2004)			0.815	0.262	0.237	0.598	0.791
Guo et al. (2018, 2019)			0.816	0.307	0.261	0.567	0.789

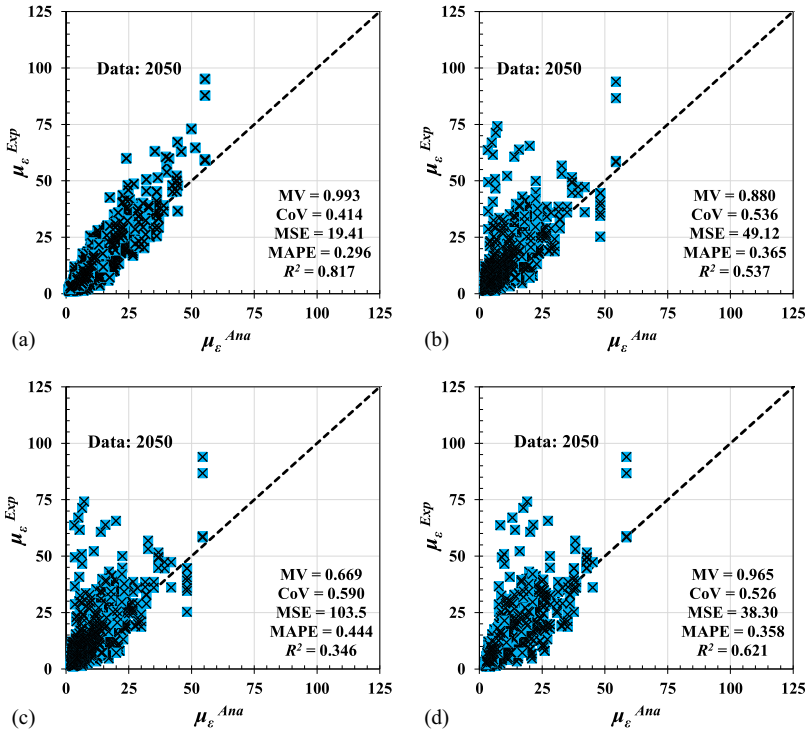

Fig. 12. Predictive performance of (a) proposed ductility model; (b) *fib* (2019); (c) CNR DT 200/2004 (CNR 2004); and (d) Guo et al. (2018, 2019).

Table 13. Statistical assessment of available unified models for predicting μ_ε

ID	Type	Test data	MV	CoV	MAPE	MSE	R^2
Proposed model	FF, FP	2,050	0.993	0.414	0.296	19.41	0.817
fib (2019)			0.880	0.536	0.365	49.12	0.537
CNR DT 200/2004 (CNR 2004)			0.669	0.590	0.444	103.5	0.346
Guo et al. (2018, 2019)			0.965	0.526	0.358	38.30	0.621

upgrading in the predictive performance of the proposed compressive strength and ductility models (Shayanfar et al. 2023c). This also rationalizes there being a continuous process of data collection and consequent recalibration of the models until convergence in terms of accuracy is reached. Moreover, this version of the proposed models does not yet comprise an available solution for implementation in the design practice, which requires consideration of the relevant safety factors and the demonstration of their validations for real scale FRP-confined RC columns. Nonetheless, owing to the general nature of the proposed methodology for the determination of f_{cc} and μ_ε, a proper foundation is provided for the establishment of predictive formulations applicable to fully or partially FRP-confined circular or noncircular RC columns, where the influence of the dual confinement mechanism of FRP wraps and steel stirrups or hoops needs to be evaluated or considered, for presentation in future publications.

Validation of the Proposed Predictive Models

This section presents the predictive performance of the proposed unified compressive strength and strain ductility models based on all the test data of FRP-confined concrete with different cross-section shapes and confinement arrangements. Furthermore, these models' performances are also compared with those associated with CNR DT 200/2004 (CNR 2004), Guo et al. (2018, 2019), and *fib* (2019) models.

Fig. 11 and Table 12 compare the predictive performance of the proposed strength model with those obtained from CNR DT 200/2004 (CNR 2004), Guo et al. (2018, 2019), and *fib* (2019) models, based on the predicted results of 2,117 test data of FFCC, FFSC, FFRC, FPCC, FPSC, and FPRC. A close agreement of the analytical and experimental results verifies the good performance of the proposed model. Furthermore, of the considered models, the obtained statistical indicators highlight the capability of *fib* (2019)'s model. Nevertheless, the proposed strength model has a superior performance in the prediction of f_{cc}.

In Fig. 12 and Table 13, the performance of the proposed ductility model in predicting μ_ε is compared with that obtained from the application of CNR DT 200/2004 (CNR 2004), Guo et al. (2018, 2019), and *fib* (2019) models. It can be seen that even though Guo et al. (2018, 2019) exhibited the best performance among the considered model, the proposed model was capable of providing considerably better predictions of 2,050 test data of FFCC, FFSC, FFRC, FPCC, FPSC, or FPRC.

Summary and Conclusions

In this study, new unified predictive formulations were developed to estimate the compressive strength (f_{cc}) and axial strain ductility (μ_ε) of circular, square, and rectangular cross-section concrete columns with either full (FFCC, FFSC, and FFRC), or partial confinement (FPCC, FPSC, and FPRC), based on a regression analysis technique. To establish a strength model, the fundamental assumption was that f_{cc} of FRP-confined concrete is significantly dependent on the confinement pressure generated by the FRP jacket at the rupture stage. For the case of a strain ductility model, a new expression with a design framework [Eq. (22)] was proposed, based on the concept of the Poisson's ratio effect, whose framework is different from the existing one [Eq. (1)]. Subsequently, based on these preliminary expressions, predictive formulations based on regression analysis were developed, whose key variables are confinement stiffness, concrete strength, and FRP ultimate tensile strain. The influences of the aforementioned variables, along with size effect, were determined using regression analysis implemented on a large experimental dataset of FFCC columns. According to the unification approach introduced by Wu and Wang (2009), by introducing the nondimensional indices of R_r, R_{ca}, and R_{sf}, the dominance degrees of sectional noncircularity, cross-sectional aspect ratio, and confinement configuration type on confinement effectiveness were evaluated using the collected test databases of FFSC, FFRC, FPCC, FPSC, and FPRC. Through statistical analysis of the influences of these variables on f_{cc} and μ_ε, unification factors (β_{UF} and α_{UF}) were derived, by which the applicability of the models are extended to the various confinement scenarios. Based on the data of FFCC, FFSC, FFRC, FPCC, FPSC, and FPRC assembled in the datasets, the predictive performances of the proposed models were evaluated, and compared with those of some existing models. For the cases of f_{cc} and μ_ε, the models suggested by *fib* (2019) and Guo et al. (2018, 2019) demonstrated the best performances among the considered models, respectively. Nevertheless, superior predictive performances were achieved through the proposed strength and ductility models based on the obtained statistical indicators.

Data Availability Statement

All data, models, and code generated or used during the study appear in the published article.

Acknowledgments

This study is a part of the project "Sticker—Innovative technique for the structural strengthening based on using CFRP laminates with multifunctional attributes and applied with advanced cement adhesives" (reference POCI-01-0247-FEDER-039755). The first author also acknowledges support provided by a FCT PhD individual fellowship 2019 (reference SFRH/BD/148002/2019).

Notation

The following symbols are used in this paper:

A_0 = regression coefficient;
A_1 = regression coefficient;
A_2 = regression coefficient;
A_3 = regression coefficient;
A_4 = regression coefficient;
A_5 = regression coefficient;

B_0 = regression coefficient;
B_1 = regression coefficient;
B_2 = regression coefficient;
B_3 = regression coefficient;
b = section dimension (shorter side of section);
E_f = FRP modulus elasticity;
f_{cc} = peak axial strength of FRP-confined concrete;
f_{cu} = ultimate axial strength of FRP-confined concrete;
f_{c0} = peak axial strength of unconfined concrete;
$f_{l,u}$ = confinement pressure at FRP ultimate tensile strain;
$f_{l,\mathrm{rup}}$ = confinement pressure at FRP rupture;
h = longer side of section;
K_L = FRP confinement stiffness;
k_h = reduction factor;
k_v = reduction factor;
k_0 = constant coefficient;
L = column height;
R_{ca} = cross-sectional aspect ratio, $R_{ca} = h/b$;
R_r = nondimensional parameter, $R_r = 2r/b$;
R_{sf} = nondimensional parameter, $R_{sf} = s_f/b$;
r = corner radius;
s_f = distance between FRP strips;
t_f = nominal thickness of FRP layer;
w_f = FRP width;
Y_1 = error index;
Y_2 = error index;
Y_3 = error index;
α_{SE} = calibration factor for size effect;
α_R = calibration factor for noncircularity;
α_{UF} = unification factor;
α_λ = calibration factor for sectional aspect ratio effect;
β_{SE} = calibration factor for size effect;
β_R = calibration factor for noncircularity;
β_{UF} = unification factor;
β_λ = calibration factor for sectional aspect ratio effect;
β_0 = calibration factor;
Δ_c = FRP confinement-induced improvements;
ε_{cu} = ultimate axial strain;
ε_{c0} = axial strain corresponding to f_{c0};
ε_{fu} = ultimate tensile strain of FRP sheet;
$\varepsilon_{h,\mathrm{rup}}$ = rupture strain of FRP jacket;
μ_ε = axial strain ductility;
ν_u = ultimate secant Poisson's ratio;
ρ_ε = rupture strain ratio of FRP jackets;
$\rho_{K,e1}$ = FRP confinement stiffness index;
ξ = calibration factor;
ξ_0 = calibration factor;
Ψ_c = FRP confinement-induced improvements; and
ψ = strain reduction factor.

References

ACI (American Concrete Institute). 2017. *Guide for the design and construction of externally bonded FRP systems for strengthening concrete structures*. ACI 440.2R-17. Farmington Hills, MI: ACI.

Bai, Y. L., J. G. Dai, and J. G. Teng. 2014. "Cyclic compressive behavior of concrete confined with large rupture strain FRP composites." *J. Compos. Constr.* 18 (1): 04013025. https://doi.org/10.1061/(ASCE)CC.1943-5614.0000386.

Baji, H., H. R. Ronagh, and C. Q. Li. 2016. "Probabilistic design models for ultimate strength and strain of FRP-confined concrete." *J. Compos. Constr.* 20 (6): 04016051. https://doi.org/10.1061/(ASCE)CC.1943-5614.0000704.

Barros, J. A., S. J. Dias, and J. L. Lima. 2007. "Efficacy of CFRP-based techniques for the flexural and shear strengthening of concrete beams." *Cem. Concr. Compos.* 29 (3): 203–217. https://doi.org/10.1016/j.cemconcomp.2006.09.001.

Barros, J. A., and D. R. Ferreira. 2008. "Assessing the efficiency of CFRP discrete confinement systems for concrete cylinders." *J. Compos. Constr.* 12 (2): 134–148. https://doi.org/10.1061/(ASCE)1090-0268(2008)12:2(134).

Cao, Y. G., C. Jiang, and Y. F. Wu. 2016. "Cross-sectional unification on the stress-strain model of concrete subjected to high passive confinement by fiber-reinforced polymer." *Polymers* 8 (5): 186. https://doi.org/10.3390/polym8050186.

Cascardi, A., F. Micelli, and M. A. Aiello. 2017. "An artificial neural networks model for the prediction of the compressive strength of FRP-confined concrete circular columns." *Eng. Struct.* 140: 199–208. https://doi.org/10.1016/j.engstruct.2017.02.047.

CNR (National Research Council). 2004. *Guide for the design and construction of externally bonded FRP systems for strengthening existing structures. CNR-DT 200*. Roma, Italy: CNR.

Dai, J. G., Y. L. Bai, and J. G. Teng. 2011. "Behavior and modeling of concrete confined with FRP composites of large deformability." *J. Compos. Constr.* 15 (6): 963–973. https://doi.org/10.1061/(ASCE)CC.1943-5614.0000230.

De Lorenzis, L., and R. Tepfers. 2003. "Comparative study of models on confinement of concrete cylinders with fiber-reinforced polymer composites." *J. Compos. Constr.* 7 (3): 219–237. https://doi.org/10.1061/(ASCE)1090-0268(2003)7:3(219).

De Oliveira, D. S., V. Raiz, and R. Carrazedo. 2019. "Experimental study on normal-strength, high-strength and ultrahigh-strength concrete confined by carbon and glass FRP laminates." *J. Compos. Constr.* 23 (1): 04018072. https://doi.org/10.1061/(ASCE)CC.1943-5614.0000912.

Eid, R., N. Roy, and P. Paultre. 2009. "Normal-and high-strength concrete circular elements wrapped with FRP composites." *J. Compos. Constr.* 13 (2): 113–124. https://doi.org/10.1061/(ASCE)1090-0268(2009)13:2(113).

Fanaradelli, T., and T. Rousakis. 2021. "Assessment of analytical stress and strain at peak and at ultimate conditions for fiber-reinforcement polymer-confined reinforced concrete columns of rectangular sections under axial cyclic loading." *Struct. Concr.* 22 (1): 95–108. https://doi.org/10.1002/suco.201900386.

Fanaradelli, T. D., and T. C. Rousakis. 2020a. "3D finite element pseudo-dynamic analysis of deficient RC rectangular columns confined with fiber reinforced polymers under axial compression." *Polymers* 12 (11): 2546. https://doi.org/10.3390/polym12112546.

Fanaradelli, T. D., and T. C. Rousakis. 2020b. "Prediction of ultimate strain for rectangular reinforced concrete columns confined with fiber reinforced polymers under cyclic axial compression." *Polymers* 12 (11): 2691. https://doi.org/10.3390/polym12112691.

fib (International Federation for Structural Concrete). 2019. *Externally applied FRP reinforcement for concrete structures*. Fib Bulletin 90, Task Group 5.1. Lausanne, Switzerland: fib.

Guo, Y. C., W. Y. Gao, J. J. Zeng, Z. J. Duan, X. Y. Ni, and K. D. Peng. 2019. "Compressive behavior of FRP ring-confined concrete in circular columns: Effects of specimen size and a new design-oriented stress-strain model." *Constr. Build. Mater.* 201: 350–368. https://doi.org/10.1016/j.conbuildmat.2018.12.183.

Guo, Y. C., S. H. Xiao, J. W. Luo, Y. Y. Ye, and J. J. Zeng. 2018. "Confined concrete in fiber reinforced polymer partially wrapped square columns: Axial compressive behavior and strain distributions by a particle image velocimetry sensing technique." *Sensors* 18 (12): 4118. https://doi.org/10.3390/s18124118.

Harajli, M. H., E. Hantouche, and K. Soudki. 2006. "Stress-strain model for fiber-reinforced polymer jacketed concrete columns." *Struct. J.* 103 (5): 672–682.

He, C., and J. J. Zeng. 2022. "Fiber-reinforced polymer-confined non-circular columns with shape modification: A comprehensive review." *Polymers* 14 (3): 564. https://doi.org/10.3390/polym14030564.

Isleem, H. F., F. Peng, and B. A. Tayeh. 2022. "Confinement model for LRS FRP-confined concrete using conventional regression and artificial neural network techniques." *Compos. Struct.* 279: 114779. https://doi.org/10.1016/j.compstruct.2021.114779.

Isleem, H. F., Z. Wang, D. Wang, and S. T. Smith. 2018. "Monotonic and cyclic axial compressive behavior of CFRP-confined rectangular RC columns." *J. Compos. Constr.* 22 (4): 04018023. https://doi.org/10.1061/(ASCE)CC.1943-5614.0000860.

Janwaen, W., J. A. Barros, and I. G. Costa. 2019. "A new strengthening technique for increasing the load carrying capacity of rectangular reinforced concrete columns subjected to axial compressive loading." *Composites, Part B* 158: 67–81. https://doi.org/10.1016/j.compositesb.2018.09.045.

Lam, L., and J. G. Teng. 2003. "Design-oriented stress–strain model for FRP-confined concrete." *Constr. Build. Mater.* 17 (6-7): 471–489. https://doi.org/10.1016/S0950-0618(03)00045-X.

Lim, J. C., and T. Ozbakkaloglu. 2014. "Stress–strain model for normal- and light-weight concretes under uniaxial and triaxial compression." *Constr. Build. Mater.* 71: 492–509. https://doi.org/10.1016/j.conbuildmat.2014.08.050.

Lin, S., Y. G. Zhao, J. Li, and Z. H. Lu. 2021. "Confining stress path-based compressive strength model of axially loaded FRP-confined columns." *J. Compos. Constr.* 25 (1): 04020077. https://doi.org/10.1061/(ASCE)CC.1943-5614.0001090.

Ma, G., C. Wu, and K. Liu. 2023. "Seismic performance of lap-spliced pre-damaged and intact concrete columns strengthened or retrofitted with UHPC and NSM." *Eng. Struct.* 277: 115431. https://doi.org/10.1016/j.engstruct.2022.115431.

Mander, J. B., M. J. Priestley, and R. Park. 1988. "Theoretical stress-strain model for confined concrete." *J. Struct. Eng.* 114 (8): 1804–1826. https://doi.org/10.1061/(ASCE)0733-9445(1988)114:8(1804).

Mirmiran, A., and M. Shahawy. 1997. "Dilation characteristics of confined concrete. *Mech. Cohesive-frict. Mater.* 2 (3): 237–249.

Nematzadeh, M., M. Mousavimehr, J. Shayanfar, and M. Omidalizadeh. 2021. "Eccentric compressive behavior of steel fiber-reinforced RC columns strengthened with CFRP wraps: Experimental investigation and analytical modeling." *Eng. Struct.* 226: 111389. https://doi.org/10.1016/j.engstruct.2020.111389.

Nisticò, N., and G. Monti. 2013. "RC square sections confined by FRP: Analytical prediction of peak strength." *Composites, Part B* 45 (1): 127–137. https://doi.org/10.1016/j.compositesb.2012.09.041.

Ozbakkaloglu, T. 2013. "Axial compressive behavior of square and rectangular high-strength concrete-filled FRP tubes." *J. Compos. Constr.* 17 (1): 151–161. https://doi.org/10.1061/(ASCE)CC.1943-5614.0000321.

Ozbakkaloglu, T., and E. Akin. 2012. "Behavior of FRP-confined normal- and high-strength concrete under cyclic axial compression." *J. Compos. Constr.* 16 (4): 451–463. https://doi.org/10.1061/(ASCE)CC.1943-5614.0000273.

Ozbakkaloglu, T., and J. C. Lim. 2013. "Axial compressive behavior of FRP-confined concrete: Experimental test database and a new design-oriented model." *Composites, Part B* 55: 607–634. https://doi.org/10.1016/j.compositesb.2013.07.025.

Ozbakkaloglu, T., and T. Vincent. 2014. "Axial compressive behavior of circular high-strength concrete-filled FRP tubes." *J. Compos. Constr.* 18 (2): 04013037. https://doi.org/10.1061/(ASCE)CC.1943-5614.0000410.

Pampanin, S., D. Bolognini, and A. Pavese. 2007. "Performance-based seismic retrofit strategy for existing reinforced concrete frame systems using fiber-reinforced polymer composites." *J. Compos. Constr.* 11 (2): 211–226. https://doi.org/10.1061/(ASCE)1090-0268(2007)11:2(211).

Pantelides, C. P., Z. Yan, and L. D. Reaveley. 2004. *Shape modification of rectangular columns confined with FRP composites*. Rep. No. UT-05.03. Utah: Utah Dept. of Transportation Research and Development Division.

Pham, T. M., and M. N. Hadi. 2014. "Predicting stress and strain of FRP-confined square/rectangular columns using artificial neural networks." *J. Compos. Constr.* 18 (6): 04014019. https://doi.org/10.1061/(ASCE)CC.1943-5614.0000477.

Raza, A., M. H. El Ouni, J. Baili, and Q. uz Zaman Khan. 2022. "Data-driven analysis on axial strength of GFRP-NSC columns based on practical artificial neural network tool." *Compos. Struct.* 291: 115598. https://doi.org/10.1016/j.compstruct.2022.115598.

Rousakis, T. C., T. D. Rakitzis, and A. I. Karabinis. 2012. "Design-oriented strength model for FRP-confined concrete members." *J. Compos. Constr.* 16 (6): 615–625. https://doi.org/10.1061/(ASCE)CC.1943-5614.0000295.

Rousakis, T. C., and I. S. Tourtouras. 2014. "RC columns of square section–passive and active confinement with composite ropes." *Composites, Part B* 58: 573–581. https://doi.org/10.1016/j.compositesb.2013.11.011.

Saleem, S., Q. Hussain, and A. Pimanmas. 2017. "Compressive behavior of PET FRP–confined circular, square, and rectangular concrete columns." *J. Compos. Constr.* 21 (3): 04016097. https://doi.org/10.1061/(ASCE)CC.1943-5614.0000754.

Shan, B., F. C. Gui, G. Monti, and Y. Xiao. 2019. "Effectiveness of CFRP confinement and compressive strength of square concrete columns." *J. Compos. Constr.* 23 (6): 04019043. https://doi.org/10.1061/(ASCE)CC.1943-5614.0000967.

Shayanfar, J., J. A. Barros, and M. Rezazadeh. 2021a. "Generalized analysis-oriented model of FRP confined concrete circular columns." *Compos. Struct.* 270: 114026. https://doi.org/10.1016/j.compstruct.2021.114026.

Shayanfar, J., J. A. Barros, and M. Rezazadeh. 2022a. "Unified model for fully and partially FRP confined circular and square concrete columns subjected to axial compression." *Eng. Struct.* 251: 113355. https://doi.org/10.1016/j.engstruct.2021.113355.

Shayanfar, J., J. A. Barros, and M. Rezazadeh. 2022b. "Cross-sectional and confining system unification on peak compressive strength of FRP confined concrete." *Struct. Concr.* 24 (1): 1531–1545. https://doi.org/10.1002/suco.202200105.

Shayanfar, J., J. A. Barros, and M. Rezazadeh. 2023a. "Analysis-oriented model for partially FRP-and-steel-confined circular RC columns under compression." *Eng. Struct.* 276: 115330. https://doi.org/10.1016/j.engstruct.2022.115330.

Shayanfar, J., J. A. Barros, and M. Rezazadeh. 2023b. "Stress–strain model for FRP confined heat-damaged concrete columns." *Fire Saf. J.* 136: 103748. https://doi.org/10.1016/j.firesaf.2023.103748.

Shayanfar, J., J. A. Barros, and M. Rezazadeh. 2023c. "Analytical model to predict axial stress-strain behavior of heat-damaged unreinforced concrete columns wrapped by FRP jacket." *Eng. Struct.* 289: 116244. https://doi.org/10.1016/j.engstruct.2023.116244.

Shayanfar, J., A. Hemmati, and H. A. Bengar. 2019. "A simplified numerical model to simulate RC beam–column joints collapse." *Bull. Earthquake Eng.* 17(2): 803–844. https://doi.org/10.1007/s10518-018-0472-z.

Shayanfar, J., H. J. Kafshgarkolaei, J. A. Barros, and M. Rezazadeh. 2023d. "Unified strength model for FRP confined heat-damaged circular and square concrete columns." *Compos. Struct.* 307: 116647. https://doi.org/10.1016/j.compstruct.2022.116647.

Shayanfar, J., M. Rezazadeh, J. Barros, and H. Ramezansefat. 2021b. "A new dilation model for FRP fully/partially confined concrete column under axial loading." In *Proc., 3rd RILEM Spring Convention and Conference (RSCC 2020) Volume 2: New Materials and Structures for Ultra-Durability 3*, pp. 435–446. Cham: Springer.

Shayanfar, J., M. Rezazadeh, and J. A. Barros. 2020. "Analytical model to predict dilation behavior of FRP confined circular concrete columns subjected to axial compressive loading." *J. Compos. Constr.* 24 (6): 04020071. https://doi.org/10.1061/(ASCE)CC.1943-5614.0001087.

Shayanfar, J., M. Rezazadeh, and J. A. Barros. 2022c. "Theoretical prediction of axial response of FRP fully/partially confined circular concrete under axial loading." In *Proc., 10th Int. Conf., on FRP Composites in Civil Engineering: Proceedings of CICE 2020/2021 10*, pp. 1439–1449. Cham: Springer.

Tariq, M., A. Khan, A. Ullah, J. Shayanfar, and M. Niaz. 2022. "Improved shear strength prediction model of steel fiber reinforced concrete beams by adopting gene expression programming." *Materials* 15 (11): 3758. https://doi.org/10.3390/ma15113758.

Teng, J. G., T. Jiang, L. Lam, and Y. Z. Luo. 2009. "Refinement of a design-oriented stress–strain model for FRP-confined concrete." *J. Compos. Constr.* 13 (4): 269–278. https://doi.org/10.1061/(ASCE)CC.1943-5614.0000012.

Teng, J. G., L. Lam, G. Lin, J. Y. Lu, and Q. G. Xiao. 2016. "Numerical simulation of FRP-jacketed RC columns subjected to cyclic and seismic

loading." *J. Compos. Constr.* 20 (1): 04015021. https://doi.org/10.1061/(ASCE)CC.1943-5614.0000584.
Triantafyllou, G. G., T. C. Rousakis, and A. I. Karabinis. 2015. "Axially loaded reinforced concrete columns with a square section partially confined by light GFRP straps." *J. Compos. Constr.* 19 (1): 04014035. https://doi.org/10.1061/(ASCE)CC.1943-5614.0000496.
Triantafillou, T. C., E. Choutopoulou, E. Fotaki, M. Skorda, M. Stathopoulou, and K. Karlos. 2016. "FRP confinement of wall-like reinforced concrete columns." *Mater. Struct.* 49(1-2): 651–664. https://doi.org/10.1617/s11527-015-0526-5.
Vincent, T., and T. Ozbakkaloglu. 2013. "Influence of concrete strength and confinement method on axial compressive behavior of FRP confined high-and ultra high-strength concrete." *Composites, Part B* 50: 413–428. https://doi.org/10.1016/j.compositesb.2013.02.017.
Wang, L. M., and Y. F. Wu. 2008. "Effect of corner radius on the performance of CFRP-confined square concrete columns: Test." *Eng. Struct.* 30 (2): 493–505. https://doi.org/10.1016/j.engstruct.2007.04.016.
Wang, W., P. R. Martin, M. N. Sheikh, and M. N. Hadi. 2018a. "Eccentrically loaded FRP confined concrete with different wrapping schemes." *J. Compos. Constr.* 22 (6): 04018056. https://doi.org/10.1061/(ASCE)CC.1943-5614.0000898.
Wang, W., M. N. Sheikh, A. Q. Al-Baali, and M. N. Hadi. 2018b. "Compressive behaviour of partially FRP confined concrete: Experimental observations and assessment of the stress-strain models." *Constr. Build. Mater.* 192: 785–797. https://doi.org/10.1016/j.conbuildmat.2018.10.105.
Wang, Y., P. Liu, Q. Cao, G. Chen, B. Wan, Z. Wei, and Y. L. Bai. 2021. "Comparison of monotonic axial compressive behavior of rectangular concrete confined by FRP with different rupture strains." *Constr. Build. Mater.* 299: 124241. https://doi.org/10.1016/j.conbuildmat.2021.124241.
Wang, Y. C., and J. I. Restrepo. 2001. "Investigation of concentrically loaded reinforced concrete columns confined with glass fiber-reinforced polymer jackets." *Struct. J.* 98 (3): 377–385.
Wei, Y., and Y. F. Wu. 2016. "Experimental study of concrete columns with localized failure." *J. Compos. Constr.* 20 (5): 04016032. https://doi.org/10.1061/(ASCE)CC.1943-5614.0000686.
Wei, Y. Y., and Y. F. Wu. 2012. "Unified stress–strain model of concrete for FRP-confined columns." *Constr. Build. Mater.* 26 (1): 381–392. https://doi.org/10.1016/j.conbuildmat.2011.06.037.
Wu, Y. F., and J. F. Jiang. 2013. "Effective strain of FRP for confined circular concrete columns." *Compos. Struct.* 95: 479–491. https://doi.org/10.1016/j.compstruct.2012.08.021.
Wu, Y. F., and L. M. Wang. 2009. "Unified strength model for square and circular concrete columns confined by external jacket." *J. Struct. Eng.* 135 (3): 253–261. https://doi.org/10.1061/(ASCE)0733-9445(2009)135:3(253).
Wu, Y. F., and Y. Wei. 2016. "Stress–strain modeling of concrete columns with localized failure: An analytical study." *J. Compos. Constr.* 20 (3): 04015071. https://doi.org/10.1061/(ASCE)CC.1943-5614.0000634.
Zeng, J. J., Y. C. Guo, W. Y. Gao, W. P. Chen, and L. J. Li. 2018. "Stress-strain behavior of concrete in circular concrete columns partially wrapped with FRP strips." *Compos. Struct.* 200: 810–828. https://doi.org/10.1016/j.compstruct.2018.05.001.
Zeng, J. J., Y. C. Guo, W. Y. Gao, J. Z. Li, and J. H. Xie. 2017. "Behavior of partially and fully FRP-confined circularized square columns under axial compression." *Constr. Build. Mater.* 152: 319–332. https://doi.org/10.1016/j.conbuildmat.2017.06.152.
Zeng, J. J., Y. Y. Ye, W. Y. Gao, S. T. Smith, and Y. C. Guo. 2020. "Stress-strain behavior of polyethylene terephthalate fiber-reinforced polymer-confined normal-, high-and ultra high-strength concrete." *J. Build. Eng.* 30: 101243. https://doi.org/10.1016/j.jobe.2020.101243.